Indonesian Throughflow transport in an eddy-resolving climate model

Socorro Margarita T. Rodrigo
Student number 6818323

Thesis submitted to the Institute for Marine and Atmospheric Research Utrecht, Utrecht University, Netherlands in partial fulfilment of the requirements for the degree of

Master of Science in Climate Physics

2022

Advisory committee:
Claudia Elisabeth Wieners, Ph.D.
Janet Sprintall, Ph.D.
Michiel Baatsen, Ph.D.

Abstract

The Indonesian Throughflow (ITF) is an important pathway in global circulation, providing a passage for warm and fresh waters from the Pacific to enter the Indian Ocean. Modelling it is a challenge: in order to resolve the narrow straits of the Indonesian seas, relatively high horizontal resolution is required; additionally, as a component of thermohaline circulation, a global or quasi-global model is required. Analysed in this study are the results of the International Laboratory for High-Resolution Earth System Prediction (iHESP) High-Resolution Model Intercomparison Project (HighResMIP) run of the Community Earth System Model version 1.3 (CESM 1.3) with nominal $0.1°$, eddy-resolving ocean resolution. In this study, we will investigate if the model captures the Indonesian Throughflow transport, interannual variability, and future trends.

A comparison is made between the modelled and observed transport through four passageways of the throughflow: the Makassar Strait, Timor Passage, Ombai Strait, and Lombok Strait. In comparison with the observations, the model underestimated winter transport; nonetheless, there is a good correspondence in the mean depth-integrated transport except in Ombai Strait for which there are $\sim$1 Sv estimations below 300 m. We also compare the geostrophic transport from observations and total transport from the model at a survey transect called the IX1. This transect is in the Indian Ocean and is often used as a proxy for total ITF transport. The yearly average of modelled transport (-11.51$\pm$6.13 Sv) across the IX1 line for the top 400 m is much higher by approximately 7 Sv than that of observed geostrophic transport (-4.88$\pm$3.50 Sv). This difference might be accounted for by Ekman transport and flow below 400 m.

The interannual variability of the tropical Pacific Ocean has a significant effect on ITF transport. Through lead-lag correlations, the ITF transport correlates significantly with the El Niño-Southern Oscillation (ENSO) from July to October. By compositing the years by ENSO phase, we see the expected weakening of transport during El Niño and strengthening during La Niña. The interannual variations in the Indian Ocean also have an effect but not with statistical significance.

Contents

List of Tables

List of Figures

Chapter 1

Introduction

1.1 Background of the study

The Indonesian Throughflow (ITF) is a pathway through the Indonesian Seas through which waters from the Pacific enter the Indian Ocean. It is the only passageway in tropical latitudes that connects ocean basins in the global ocean. As such, it regulates the meridional overturning of the Indian and Pacific Oceans and is a component of global thermohaline circulation.

The ascending branch of the atmospheric Walker Circulation associated with strong convection is located above the Indonesian Seas. This position gives the seas a significant role in the climate system. Collocated with these areas are the western SST anomalies associated with El Niño-Southern Oscillation (ENSO) and the eastern sea surface temperature (SST) anomalies associated with the Indian Ocean Dipole (IOD). Surface winds are affected by such SST variations which can then shift the centre of atmospheric deep convection and influence precipitation and ocean circulation in the Indo-Pacific. The impact of the ITF can thus be felt across vastly separated regions through teleconnections with the Pacific and Indian Oceans.

Regarding the ITF, questions remain about physical process, mean circulation, and projected change under the effects of global warming. Numerical models have been used to investigate these issues and have encountered obstacles such as the relatively high horizontal resolution required to capture the narrow straits of the Indonesian seas and the complex bathymetry. The goal of this study is to analyse how well the high-resolution iHESP CESM1.3 model captures the transport of the ITF.

1.2 Research questions

Specifically, we aim to answer the following questions:

- How well does the model capture the total transport and the transport within major passageways within the Indonesian seas?
- How well does the model capture the interannual variability of the ITF, specifically in relation with the El Niño-Southern Oscillation and Indian Ocean Dipole?
- How well does the model capture the ITF's present-day climatology and what are its future trends?

Chapter 2

Review of Related Literature

2.1 Background on ITF transport

The first estimate of the strength of the ITF was published by Wyrtki, 1961 who described the seasonal flow patterns in the seas around Indonesia. Since the 1960s, there have been various attempts to estimate the transport of the ITF using observations. The most comprehensive of these was conducted from late 2003 to early 2007 called the International Nusantara Stratification and Transport Program (INSTANT). Simultaneous measurements were conducted at the major passageways of the ITF and the total transport into the Indian Ocean was estimated to be 15 Sv during the three-year period (Sprintall et al., 2009).

2.1.1 ITF passageways

The largest Indonesian seas are the following: the shallow Java Sea in the west; the shallow Arafura Sea in the East; and among the internal seas are the deeper Flores, Banda and Timor Seas. (see Fig. 2.1). To the east of Kalimantan and south of the Philippines is the Sulawesi or Celebes Sea. The West Pacific borders this sea and, towards the southeast, the Molucca/Maluku and Halmahera Seas as well.

The main pathways of the ITF were identified during the 1993-1998 "Arlindo" project which stands for Arus Lintas Indonesia, meaning "throughflow" in Bahasa Indonesian (Gordon and Fine, 1996, Ilahude and Gordon, 1996). Water from the Pacific takes two major routes on its way to the Indian Ocean: the western and eastern routes. The western route is through the Sulawesi Sea then the Makassar Strait where there is a 680 m Dewakang Sill (Fig. 2.2). Only upper thermocline and surface waters from the North Pacific then enter the Flores Sea and proceed to the

Banda Sea or exit directly to the Indian Ocean through the Lombok Strait with sill depth of ~300 m and width of ~35 km.

The eastern entryway is through the Halmahera and Maluku Seas and over the ~1940 m sill of the Lifamatola Strait. These waters are composed of North Pacific upper water and also saltier, lower thermocline and intermediate South Pacific water (Gordon and Fine, 1996, Ffield and Gordon, 1992, Bray et al., 1996).

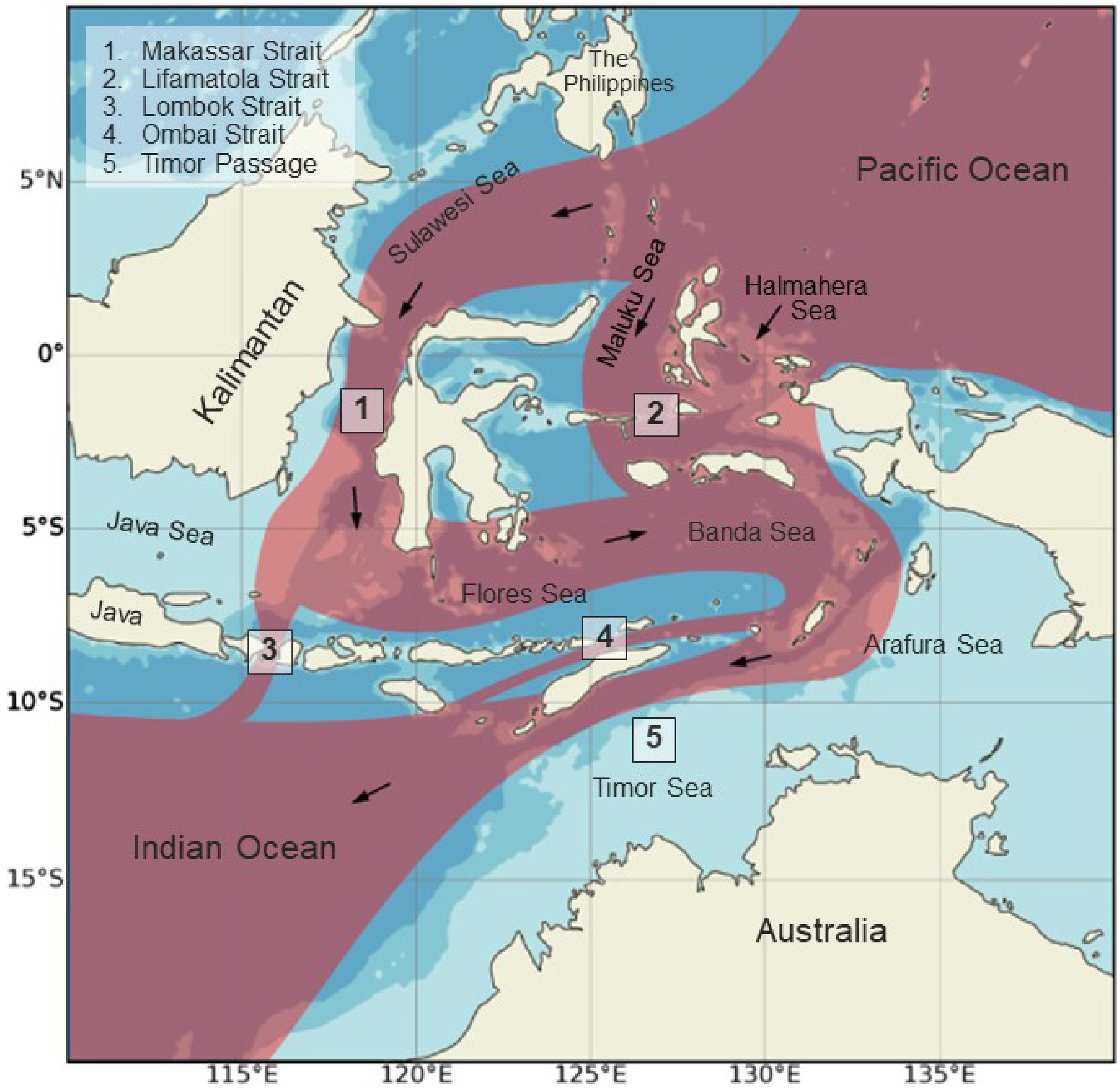

Figure 2.1: Map of the Maritime Continent, largest Indonesian Seas, and a schematic representation of the Indonesian Throughflow pathways.

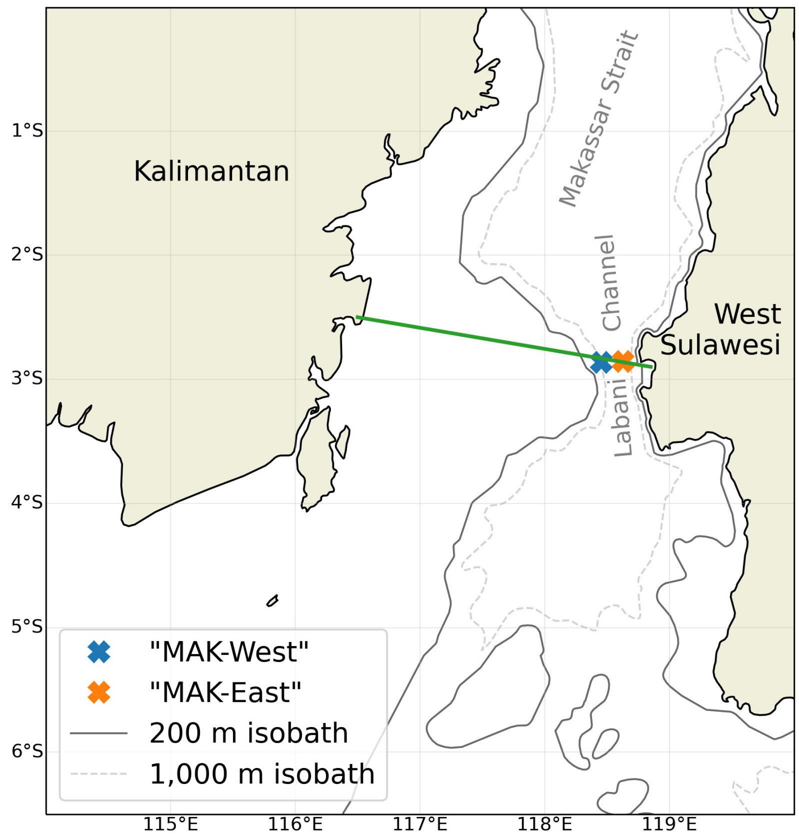

Figure 2.2: The Makassar Strait with 200 m and 1000 m isobaths, showing that Labani Channel is the narrowest constriction. Within it, the Dewakang Sill is ∼680 m deep. The two moorings MAK-West and MAK-East are marked with crosses. The green line is the chosen model transect for calculating transport.

2.1.2 Makassar Strait

The westernmost deep pathway is the Makassar Strait (2.2) with a sill depth of ∼680 m at the Labani Channel which is ∼45 km wide at 50 m depth. Within the channel, two moorings were deployed within the Arlindo Circulation program from late 1996 to mid-1998. This moored time series was continued during INSTANT from 2004-2006 and afterwards by the MITF or the Monitoring of the ITF project from 2006 onward. Fig. 2.2 shows the two moorings, "MAK-West" (2°51.9'S, 118°27.3'E) and "MAK-East" (2°51.5'S, 118°37.7'E). Not including the gaps in measurement, the data amounts to 13.3 years of monitoring (Gordon et al., 2019).

The transport through the Makassar Strait averages 12-13 Sv or approximately 77% of the ITF. The time series is able to reveal fluctuations on different timescales, including the interannual scale of ENSO and the IOD (Gordon et al., 2019).

2.1.3 Lombok Strait, Ombai Strait, and Timor Passage

Eleven moorings were deployed as part of INSTANT from January 2003 to December 2006. They are divided among the inflow passages (the aforementioned Makassar Strait and Lifamatola Strait) and three major outflow passageways: Lombok Strait, Ombai Strait, and Timor Passage. The measurements were full-depth in-situ velocity, temperature, and salinity profiles of the ITF. The Lombok Strait is a narrow passageway of ∼35 km width and a sill depth of ∼300 m, located between the islands of Bali and Lombok, through which ∼2.6 Sv of ITF waters pass (Fig. 2.3). The Ombai Strait is approximately the same width, ∼35 km, and has an upstream sill depth of ∼1450 m in Alor Strait at ∼2450 m in Wetar Strait (Fig. 2.4). This passageway is between Alor and Timor-Leste and approximately 5 Sv is transported through it. Lastly, the width of Timor Passage is ∼160 km, an order of magnitude higher. However, as seen in Fig. 2.5, most of the passage is less than 200 m deep and thus the INSTANT moorings were located in a narrow, deep constriction to the west. It has an eastern sill depth of ∼1250 m at Leti Strait and western sill depth of ∼1890 m and approximately 7.5 Sv passes through it (Sprintall et al., 2009).

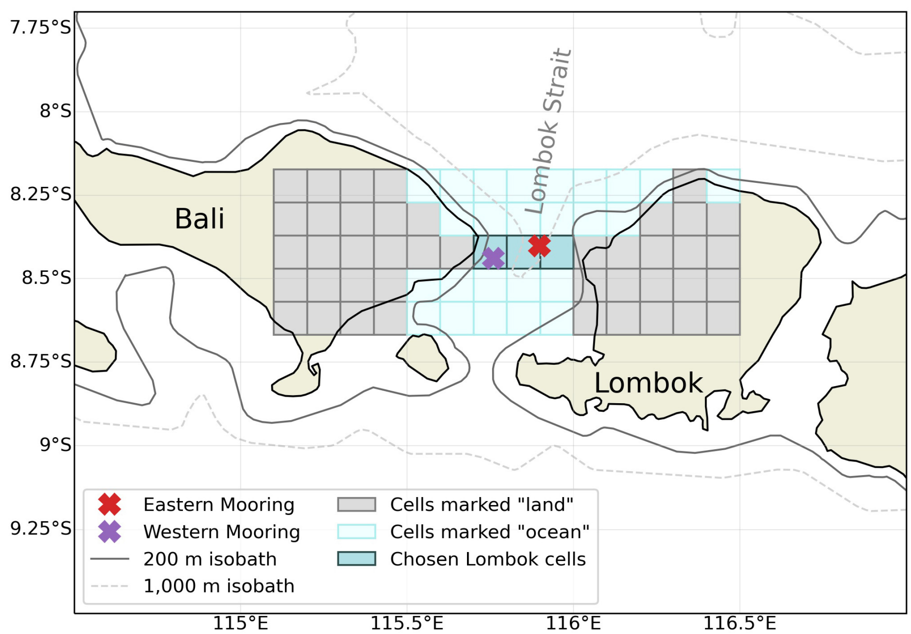

Figure 2.3: The Lombok Strait with 200 m and 1000 m isobaths. The two moorings, "Eastern" and "Western" are marked with crosses. In order to show the model resolution, the cells are plotted here where grey boxes indicate those designated as land and light blue as ocean. The dark blue cells are the chosen model grid cells which compose the transect used for this study.

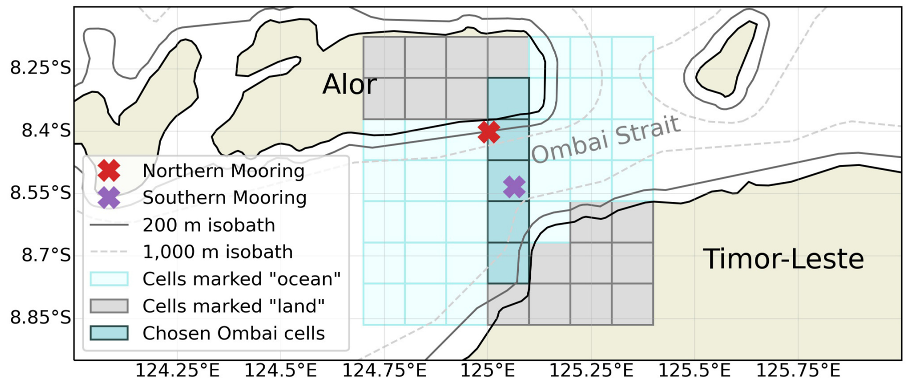

Figure 2.4: The Ombai Strait with 200 m and 1000 m isobaths. The two moorings, "Northern" and "Southern" are marked with crosses. In order to show the model resolution, the cells are plotted here where grey boxes indicate those designated as land and light blue as ocean. The dark blue cells are the chosen model grid cells which compose the transect used for this study.

2.1.4 The expendable bathythermograph transect, "IX1"

A program from 1983 until the present conducts expendable bathythermograph (XBT) surveys from ships of opportunity along what's called the "IX1" line (Fig. 2.6). This line connects Freemantle, Western Australia, and the Sunda Strait, Indonesia. The transect is repeated roughly 18 times a year with XBT profiles obtained every 50–100 km which measure temperature down to depths of 400 or 700 m. The route has been chosen to effectively sample the ITF flow and can be used as a proxy for total ITF transport into the Indian Ocean. These surveys are operated by Australia's Commonwealth Scientific and Industrial Research Organisation (CSIRO), Bureau of Meteorology (BOM), Integrated Marine Observing System (IMOS), and with assistance from the National Oceanic and Atmospheric Administration (NOAA) (Q.-Y. Liu et al., 2015, Australian Research Data Commons, 2022, Ridgway et al., 2013).

The waters from the Makassar Strait travel to the Banda Sea where they have a residence time of approximately 1 year. They experience strong vertical mixing before they are exported to the Timor Sea (Gordon et al., 2010). From the Makassar Strait to the IX1 line, models have predicted a journey of 2-3 years (Song et al., 2004). The flow through the Makassar Strait influences the westward transport at the IX1 line and thus the heat transport into the Indian Ocean (Gordon et al., 2019).

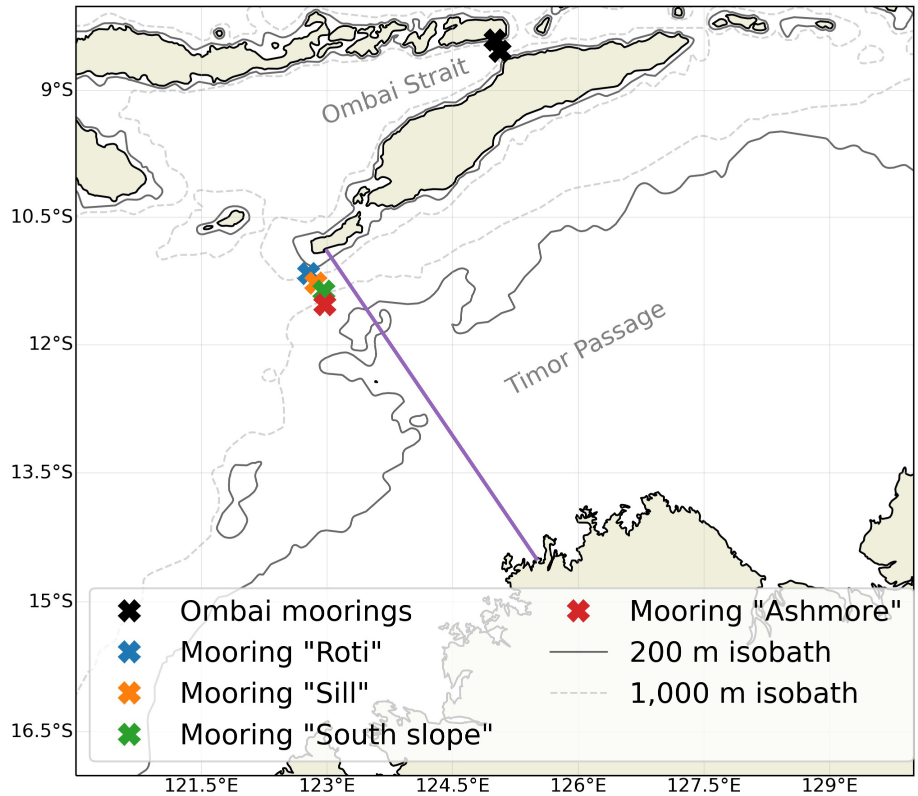

Figure 2.5: The Timor Passage with 200 m and 1000 m isobaths. The deepest region of the Timor Passage is the Timor Trough to its north. The four moorings, "Roti," "Sill," "South slope," and "Ashmore" are marked with crosses. Indicated in black are also the moorings of the Ombai Strait.

2.2 Influence of ENSO and IOD on the ITF

The ITF, through its volume, heat, and freshwater transfer, affects the Pacific and Indian Oceans and thus regional sea-air interactions and precipitation patterns over various timescales (e.g., Godfrey, 1996, Potemra and Schneider, 2007, Lee and McPhaden, 2008, Tokinaga et al., 2012). Likewise, winds in the Pacific and Indian Oceans affect the ITF. On average, Pacific trade winds cause higher sea levels in the western tropical Pacific and the ITF is driven by a pressure gradient between the Pacific and Indian Oceans on time scales of a year and longer (Wyrtki, 1987). The sea levels in the ITF exit region in the southeast Indian Ocean is regulated by the monsoons. The pressure gradient is heavily affected by ENSO and IOD.

The ENSO, a dominant mode of interannual climate variability, is characterised by sea surface temperature anomalies (SSTAs) in the equatorial Pacific. A positive mode or El Niño is characterised by positive SSTA in the eastern equatorial Pacific,

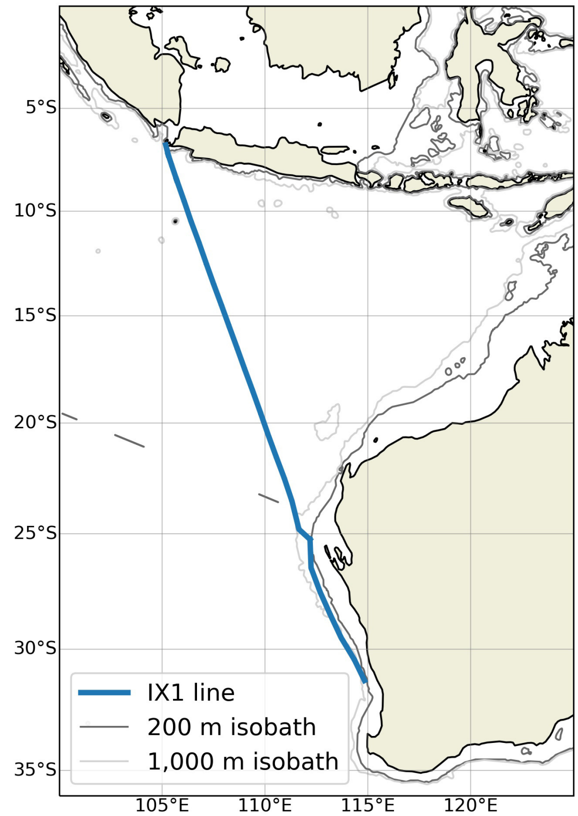

Figure 2.6: The IX1 transect used for this study, based on the locations of repeated expendable bathythermograph profiles taken from 1984-2015.

as westward trade winds decrease in strength. A negative mode or La Niña is characterised by the opposite, negative SSTA in the eastern equatorial Pacific as trade winds are stronger.

The Indian Ocean Dipole is a mode of SSTA variability as well, although smaller in spatial scale than the ENSO. A negative IOD phase is when the normal surface winds which blow to the east intensify and strengthen the gradient of anomalously warm waters to the east and cool in the west. A positive IOD occurs when westerly surface winds weaken and sometimes reverse in direction, and waters towards Africa are anomalously warm while waters near Indonesia become anomalously cool (Saji et al., 1999). The ENSO and IOD often coincide and influence each other, with a positive IOD phase often occurring in the boreal autumn of an El Niño developing year and similarly, a negative IOD phase with a La Niña. ENSO is thought to affect the whole lifespan of the IOD but the IOD mainly influences the developing phase of ENSO (Yuan and Li, 2008).

It has been suggested by models and observations that the ITF weakens during

El Niño phases as trade winds are relaxed or reversed and thus sea level heights in the western Pacific are lower. During the La Niña, the opposite conditions prevail: the sea level heights are higher in the western Pacific as trade winds strengthen and the ITF is stronger (Clarke and Liu, 1994, Meyers, 1996, Gordon et al., 1999). The ITF transport anomalies are due to radiated Rossby waves and coastal Kelvin waves forced by ENSO winds (S. Wijffels and Meyers, 2004). Thus, the speed of these processes cause a lag of approximately 9 months in the response of the ITF to ENSO (England and Huang, 2005). The positive IOD phases which often coincide with El Niño are characterised by anomalously cool waters and lower sea levels towards Indonesia, which strengthens the flow of the ITF; meanwhile, the negative IOD phase often coinciding with La Niña is characterised by higher sea levels toward Indonesia which would weaken its flow (Sprintall and Révelard, 2014, Potemra and Schneider, 2007). Immediately or within 5 months, the ITF transport anomalies respond to the IOD which observations suggest result from Kevin waves sourced at the equator (Sprintall et al., 2009, S. Wijffels and Meyers, 2004). The individual effects of the IOD and ENSO on the ITF are difficult to resolve as they can counteract each other. However, the duration of an IOD phase is often shorter than its ENSO counterpart as both phases usually begin in boreal spring and come winter, the IOD terminates while the ENSO peaks; thus, the ENSO influence on the ITF transport anomalies should dominate for longer (Wang, 2019).

2.3 Model description

Community Earth System Model version 1.3 or CESM1.3 was developed by the US National Center for Atmospheric Research (NCAR) in collaboration with other groups and was validated with a 100-year simulation. The component models are the Community Atmosphere Model version 5, the Parallel Ocean Program version 2, the Community Ice Code version 4, and the Community Land Model version 4 (iHESP, 2022b).

This study will utilise the CESM1.3 simulation of iHESP or the "International Laboratory for High-Resolution Earth System Prediction". iHESP combines the expertise of three institutions: Qingdao National Laboratory for Marine Science and Technology (QNLM), Texas A&M University (TAMU), and NCAR. This group based their work on a CESM 1.3 version named *CESM1.3-beta17_sehires20* described in Meehl et al., 2019 which was originally designed for a 0.25° degree atmosphere and nominal 1° ocean model. They configured a higher resolution version with a nominal

0.1° or approximately 10 km resolution in the ocean and sea-ice. At this resolution, ocean eddies are resolved.

They performed a historical and future simulation which spanned from 1850–2100. A pre-industrial control simulation kept constant at 1850 conditions and run for 250 years, was used as a starting point. For the succeeding years, 1850–2005, historical forcing was used. From 2006-2100, the representative concentration pathway 8.5 (RCP8.5) forcing was used in accordance with CMIP5 (Coupled Model Intercomparison Project Phase 5) protocol: RCP8.5 assumes no policy-driven mitigation against greenhouse gas emissions, allowing their increase such that $\sim$1370 ppm CO_2-equivalent concentrations are reached by 2100. This is called the 250-year high-resolution 1850 transient simulations or "historical and future transient" climate. The iHESP runs are unprecedented as simulations which were performed before this and were similar in resolution had shorter integration lengths (iHESP, 2022a).

Chapter 3

Methodology

3.1 CESM 1.3 output

Ocean variables were downloaded as NetCDF files from the iHESP CESM1.3 historical and future transient simulations.[1] The following variables were of interest: the u– and v–velocities for the transport calculations and the sea surface temperatures to compute the ONI and DMI of the model.

The model was initialised with 1850 pre-industrial conditions. From 1850–2005, historical forcing was used while from 2006–2100, RCP8.5 forcing was used in compliance with CMIP5 experimental protocol. The observations are not expected to correspond year-by-year with CESM output, such as their respective ENSO and IOD phases: as a fully-coupled climate simulation, the winds and ocean conditions are forced with historical radiative balance and greenhouse gas emissions, but not winds. Thus, the ENSO and IOD which are chaotic systems will not coincide with the historical phases. Nonetheless, they can be compared statistically: as such, we will compare their seasonal averages and interannual behaviour with respect to their corresponding ONI and DMI indices.

3.2 Volume transport calculation from model

The volume transport perpendicular to a transect, Q is computed as follows,

$$Q = \int \int U \, dx \, dz \tag{3.1}$$

[1] https://ihesp.github.io/archive/products/ihesp-products/data-release/DataRelease_Phase2.html

with U being the velocities perpendicular to the transect, z integrated over a section of depth, and x as the distance along the transect (Eq. 3.1). By convention, negative values of volume transport in the ITF are towards the Indian Ocean while positive are towards the Pacific Ocean (See Figs. 2.1 and 3.1 as reference).

The model years from 1960-2015 are selected to represent transient conditions similar to the present. Transport is also computed for the last 30 years of the model, 1970-2100.

CESM output and observational data of ITF transport is strongly seasonal as the flow is forced heavily by the boreal summer and winter monsoons. When such seasonal cycles must be removed, a simple method is used: the transport anomaly was computed with respect to the averages of the corresponding month. For example, January averages for 1960-2015 are subtracted from the January of a certain year.

3.3 Volume transport in observational data

Passageway	Time Period	Total # of months
IX1	1984-2015	384
Makassar Strait	2004-2011 2013-2017	141
Lombok Strait Ombai Strait Timor Passage	2004-2006	36

Table 3.1: The five passageways for which transport is computed: the IX1, Makassar Strait, Lombok Strait, Ombai Strait, and Timor Passage. Indicated in the 2nd column are the years for which observations were available and in the third column, the corresponding total number of months.

The total transport computed from the model is from u– and v– velocities which corresponds directly with the observed transport through four of five transects considered in this study: Makassar Strait, Lombok Strait, Ombai Strait, and Timor Passage. The longest measurement period of the four is the Makassar Strait for which moorings were deployed during the INSTANT and MITF campaigns (Tab. 3.1). The data from Lombok Strait (Fig. 2.3), Ombai Strait (Fig. 2.4), and Timor Passage (Fig. 2.5) all span from 2004-2006 as they are all from the INSTANT program (Tab. 3.1).

The fifth transect considered was the IX1, chosen as it is a proxy for total ITF transport that enters the Indian Ocean. The available observational volume transport data was from 1984-2015, derived from XBT measurements from the surface to 400

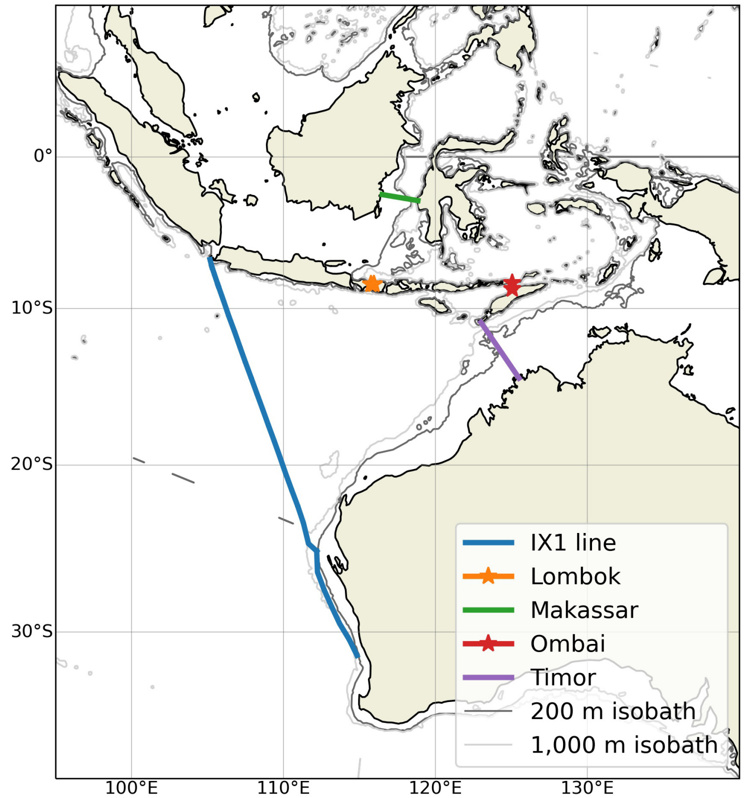

Figure 3.1: Five transects are selected for the computation of transport. The IX1, in blue is a proxy for total ITF transport. Makassar is a major inflow strait while Lombok, Ombai, and Timor are three major outflow passages. All transects have observations with which we can compare transport.

m depth, collected by Australia's CSIRO and BOM. These surveys encompass the largest time span of all transport datasets (Tab. 3.1). The geostrophic transport could be calculated from such measurements as the IX1 line is in the open ocean. However, we compare this geostrophic transport to total transport computed from model velocities, which is a limitation of this study as it would be more apt to compute and compare it with the geostrophic velocities from the model. The five transects are plotted together in Fig. 3.1.

3.4 CESM 1.3 ONI and DMI calculations

3.4.1 ONI

The Oceanic Niño Index is based on sea surface temperature anomalies (SSTA) in the Niño 3.4 region (170°W – 120°W, 5°S – 5°N). The ONI uses a 3-month running mean of SSTAs with respect to a base period of 30 years centred around the year because of significant warming trends in the Niño 3.4 region since 1950. The seasonal cycle is effectively removed by computing SSTA with respect to the same month within the 30-year base period: January averages from the base period are subtracted from the 3-month running mean for January of a certain year, and so on for the other months. The operational definition of an El Niño is when the anomalies exceed +0.5°C and La Niña, -0.5°C for at least five consecutive months. The observationally-based ONI product was downloaded from the dataset of Trenberth, K. & National Center for Atmospheric Research Staff, 2020.[2] The same definition is used when the ONI was computed from the iHESP CESM1.3 model.

3.4.2 The Dipole Mode Index

The index of the Indian Ocean Dipole is named the "DMI" or Dipole Mode Index and defined as the difference between SST anomalies between the western (50°E – 70°E, 10°S – 10°N) and southeastern (90° E – 110°E, 10°S – 0°) Indian Ocean. Unlike the ONI, the DMI is not computed as a 3-month average; however, similar to the ONI, the seasonal cycle is removed by computing the anomaly with respect to the mean of corresponding months within the base period of 30 years. Positive DMI means warm anomalies in the west and cool in the east; and negative IOD would be the opposite. Operationally, a positive (negative) IOD phase occurs when the DMI is +0.4°C or higher (-0.4°C or lower) for at least three consecutive months. The DMI is computed from the iHESP CESM1.3 model using this definition.

The observationally-based DMI product from SST observations was made available by NOAA Earth System Research Laboratory (ESRL)[3] and calculated using the Reynolds OIv2 SST analysis (Optimum Interpolation Sea Surface Temperature V2).

[2] https://climatedataguide.ucar.edu/climate-data/nino-sst-indices-nino-12-3-34-4-oni-and-tni
[3] https://stateoftheocean.osmc.noaa.gov/sur/ind/dmi.php

Chapter 4

Results and Discussion

4.1 ITF transport

4.1.1 The inflow passageway, Makassar Strait

The observed transport in the Makassar Strait is bimodal, peaking two months of the year, in March (-14.09 Sv) and in August (-15.60 Sv) as seen in Fig. 4.1. The weakest transport occurs in November on average (-7.29 Sv). On the other hand, the model shows a single peak with a maximum in July of -12.48 Sv and a low of -1.33 Sv in December. The overlap of the two shaded regions indicating one standard deviation from the mean occurs from April to November, while the model most heavily underestimates the transport from December to March. The yearly averages show model underestimation which is most pronounced in boreal winter: the observational average is -12.21±3.30 Sv and the model -8.45±4.25 Sv (Tab. 4.1). In terms of the predicted Makassar transport at the end of the 21st century, the monthly averages follow a similar distribution as the 1960–2015 transport, but the model mean is lower by 2.51 Sv to 4.60 Sv. In the months of December and January, the Makassar transport is even positive or towards the Pacific Ocean (1.17 Sv in December, 1.12 Sv in January).

Samanta et al., 2021 look into the effect of the projected Makassar Strait slowdown on the South China Sea (SCS) climate with the use of three HighResMIP models. The multi-model ensemble of the results were analysed for mass and heat transport during the future projection (2015–2100) where the SSP5-585 scenario was applied, which is equivalent to the RCP8.5. Heat transport in both Makassar and Lombok Straits are predicted to decrease by up to ∼55% and ∼75%, respectively. This will be accompanied by a higher wintertime heat transport by Karimata Strait (∼11%)

	IX1 (0-400 m)	Makassar	Lombok	Ombai	Timor
Model (Sv) 1960-2015	-11.51±6.13	-8.45±4.25	-2.30±1.67	-3.80±1.31	-7.97±3.68
Model (Sv) 2070-2100	-8.31±6.09	-5.08±4.07	-1.93±1.38	-1.19±1.28	-4.88±3.78
Observations (Sv)	-4.88±3.50	-12.21±3.30	-2.60±1.42	-5.18±2.26	-7.36±2.15

Table 4.1: Average volume transport and standard deviation (Sv) per transect, negative being in the direction of the Indian Ocean. The average is computed over all available observations and for the model, the average is taken from conditions like the present, 1960-2015, and the future, 2070-2100.

which might increase its importance in the future. Nonetheless, heat content in the SCS is expected to increase by the end of the century.

4.1.2 The three outflow passageways, Timor Passage, Lombok Strait, and Ombai Strait

Observational data from Timor Passage, Lombok Strait, and Ombai Strait all span three years which are sufficient to show some seasonality. As with Makassar Strait, the observations at Timor Passage (Fig. 4.2) show two peaks where the highest is in March (-10.02 Sv) and the second in October (-8.22 Sv). The two troughs occur in August (-5.38 Sv) and December (-5.08 Sv). The model shows some bimodal behaviour but its two peaks are of similar magnitudes and closer to boreal summer: May (-11.58 Sv) and September (-10.19 Sv). The weakening of the flow in January to March is exaggerated by the model while the May to November flow is overestimated. On average, the model overestimates the flow by 0.61 Sv, where the model average is -7.97±3.68 and the observations, -7.36±2.15.

It should be noted that only three model cells composed the Lombok Strait transect (Fig. 2.3) and five grid cells for Ombai Strait (Fig. 2.4), both of which are approximately 35 km wide and model resolution is ∼10 km. Ombai Strait has two grid cells more due to the orientation of the transect.

The Lombok Strait observations (Fig. 4.3) peak in August (-4.46 Sv) and reach their lowest value in December (-1.61 Sv) although it has three small peaks in total. Perhaps a three-year period was not enough to show the seasonality in this strait well. In contrast, the longer time series from the model output had two peaks: one in April (-2.91 Sv) and in July (-4.13 Sv). The winter weakening was stronger in the model

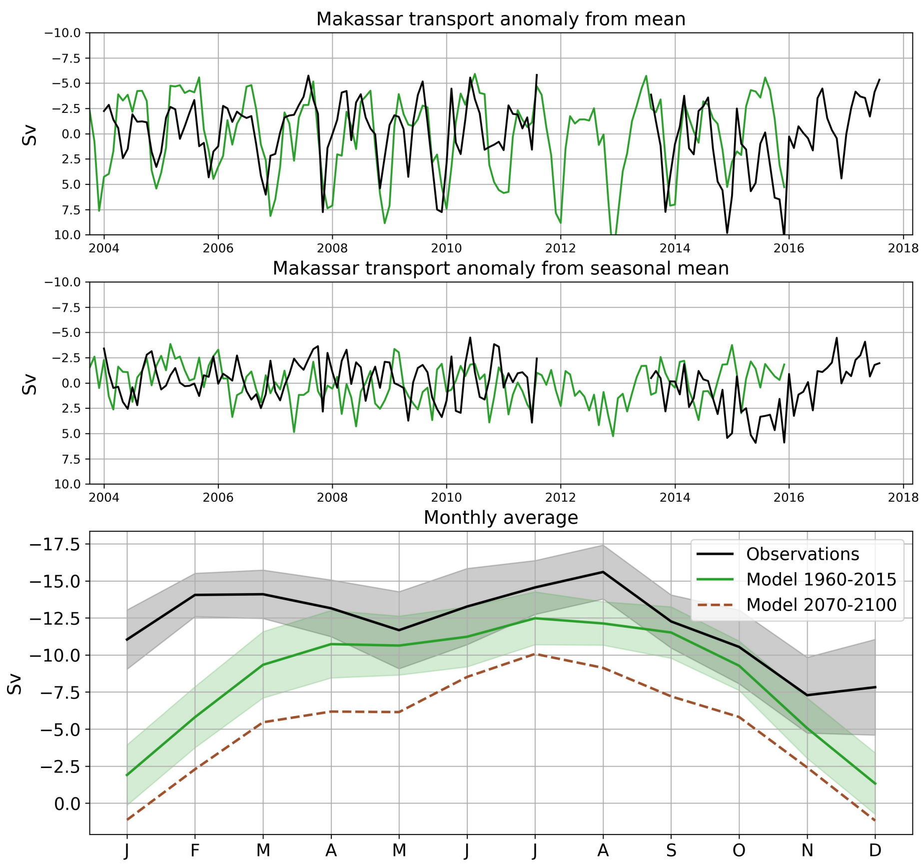

Figure 4.1: Makassar Strait volume transport: observational data from 2004-2006 is plotted in black while the model transport from 1960-2015 is in green for the (top) anomaly from the mean and (middle) anomaly from seasonal mean. The bottom plot shows monthly averages of these timeseries: model data from 1960-2015 is in green, the observations are in black, and one standard deviation is in plotted as shaded regions, while the model data from 2070-2100 is a brown dashed line.

than in observations, with a flow reversal in December (0.70 Sv). The model average (-2.30±1.67) is very close to the observations (-2.60±1.42). Because the observational and model averages per month are within a standard deviation of the other for 10 out of 12 months, the model seems to estimate the transport magnitude well (Tab. 4.1).

In observations, the full Ombai Strait transport peaks in boreal winter (January: -7.70 Sv) and summer (July: -6.88 Sv, June: -6.70 Sv, Aug: -5.90 Sv). The flow is weakest in September (-2.55 Sv) and May (-2.64 Sv). The modelled summer transport is lower with a June peak of -4.89 Sv. September is another local maximum of -4.44 Sv and the observed winter strengthening is reflected by a small peak in December of -4.30 Sv. On average, the model underestimates the transport by 1.38 Sv with the

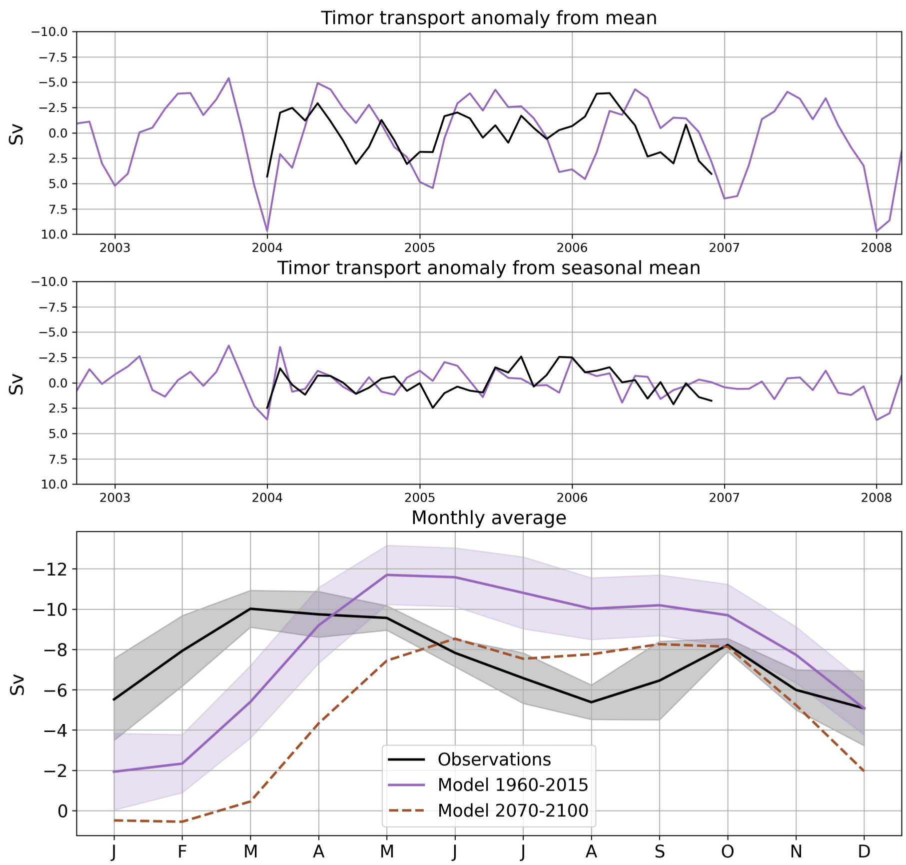

Figure 4.2: Timor Passage volume transport: observational data from 2004-2006 is plotted in black while the model transport from 1960-2015 is in purple for the (top) anomaly from the mean and (middle) anomaly from seasonal mean. The bottom plot shows monthly averages of these timeseries: model data from 1960-2015 is in purple, the observations are in black, and one standard deviation is in plotted as shaded regions, while the model data from 2070-2100 is a brown dashed line.

model average of -3.80±1.31 and observational average of -5.18±2.26.

A study by X. Feng et al., 2013 used a LICOM2.0 model and found significant flow near 900 m in the Ombai Strait. The average model transport from the top 300 meters, -2.90±1.15 Sv and from the full water column, -3.80±1.31 Sv (Tab. 4.1) gives 0.90 Sv transport below 300 m. In the observations, the difference is 1.89 Sv and thus the model underestimates the transport below 300 m by ∼1 Sv.

In summary, the modelled Timor Passage yearly transport is very close to that of the observations, despite stronger transport in summer and weaker transport in winter. The modelled Lombok Strait transport overlaps with the observed monthly transport for 10 out of 12 months, and the average yearly values are very close (only a difference of 0.3 Sv). Lastly, the Ombai Strait transport is underestimated by the model by only 1.38 Sv which may be accounted for by underestimations below 300

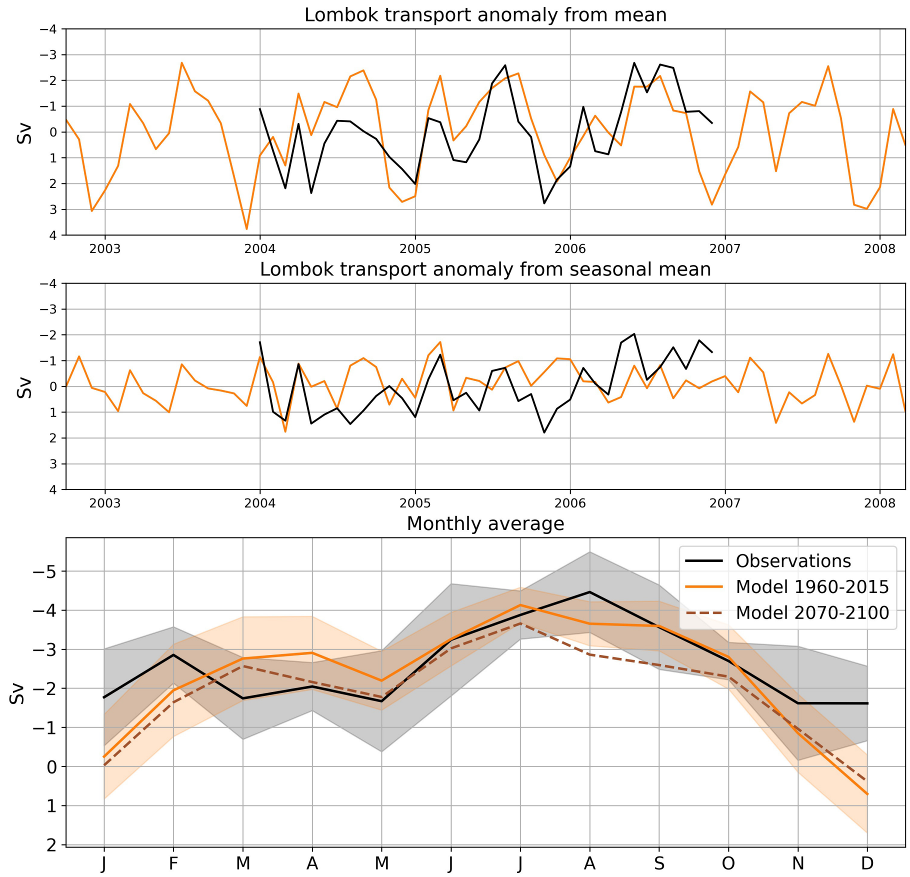

Figure 4.3: Lombok Strait volume transport: observational data from 2004-2006 is plotted in black while the model transport from 1960-2015 is in orange for the (top) anomaly from the mean and (middle) anomaly from seasonal mean. The bottom plot shows monthly averages of these timeseries: model data from 1960-2015 is in orange, the observations are in black, and one standard deviation is in plotted as shaded regions, while the model data from 2070-2100 is a brown dashed line.

m. Therefore, we can say that the transport through the outflow passageways is captured well by the model in comparison with these three years of observations from INSTANT.

4.1.3 Transport across the IX1 line

IX1 observations (Fig. 4.5) for the geostrophic flow in the top 400 m peak twice: once in March (-5.83 Sv) and once in September (-8.75 Sv), with two troughs in June (-2.25 Sv) and December (-2.40 Sv). The model transport calculated from u- and v-velocities is much higher in magnitude. Its two peaks are closer together, temporally and in magnitude: July (-20.41 Sv) and September (-17.93 Sv). The

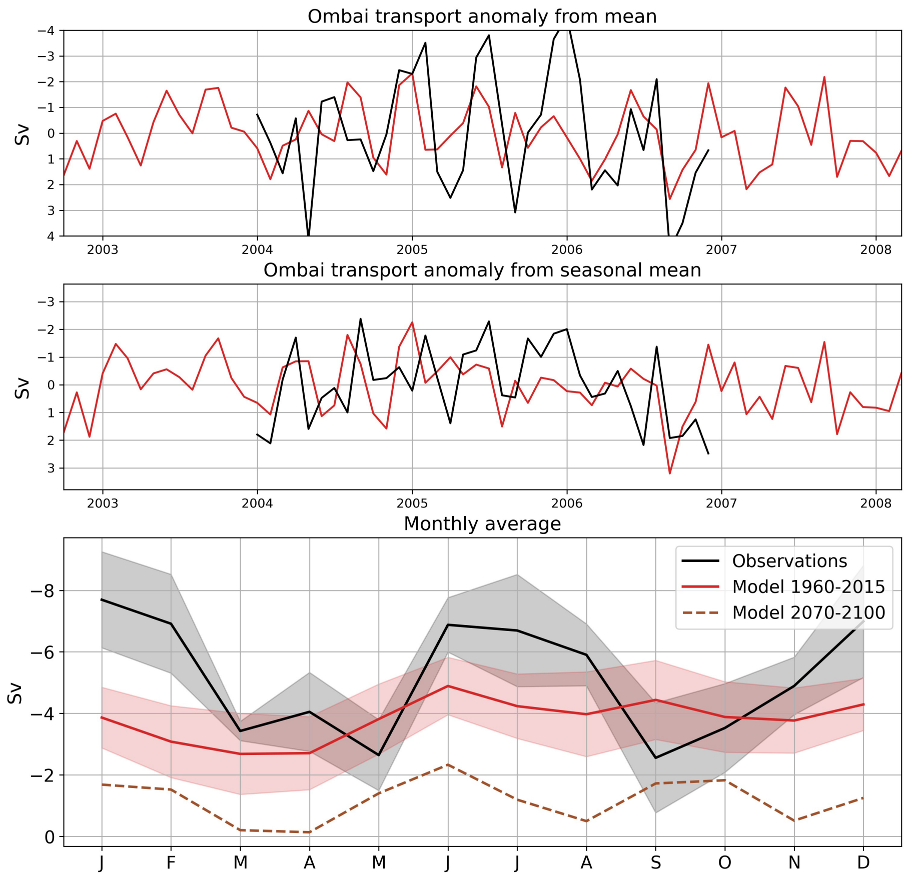

Figure 4.4: Ombai Strait volume transport: observational data from 2004-2006 in black and the model transport from 1960-2015 in red for the (top) anomaly from the mean and (middle) anomaly from seasonal mean. The bottom plot shows monthly averages of these timeseries: model data from 1960-2015 is in red, the observations are in black, and one standard deviation is in plotted as shaded regions, while the model data from 2070-2100 is a brown dashed line.

weakest transport occurs in the month of December (-5.39 Sv). The 1960-2015 model average is -11.51±6.13 Sv while the observations has an average of -4.88±3.50.

In this section and the next (Section 4.1.4), we discuss how this large difference may be accounted for mostly by Ekman transport and model underestimations of transport below 400 m. However, we also show how the modelled transport of the outflow passageways and the IX1 are self-consistent: the sum of the outflow passageways matches the total transport across the IX1 line. Thus, the IX1 modelled total transport may be trusted as a proxy for total ITF transport as it has been shown in the previous section that the individual outflow passageways are captured relatively well (Section 4.1.2).

From the estimates of S. E. Wijffels et al., 2008, the geostrophic transport across

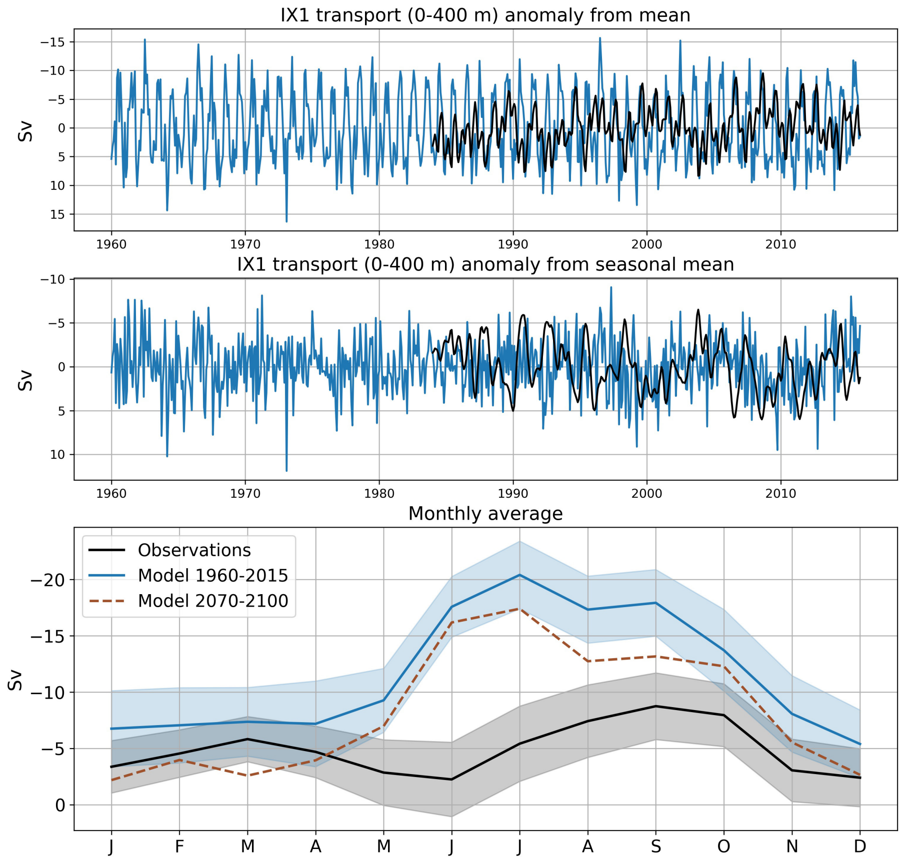

Figure 4.5: IX1 volume transport in the top 400 m: observational data from 1984-2015 is plotted in black while the model transport from 1960-2015 is in blue for the (top) anomaly from the mean and (middle) anomaly from seasonal mean. The bottom plot shows monthly averages of these timeseries: model data from 1960-2015 is in blue, the observations are in black, and one standard deviation is in plotted as shaded regions, while the model data from 2070-2100 is a brown dashed line.

the IX1 line from 0-750 m is 5.2±1.5 Sv, which means ∼0.32 Sv geostrophic transport occurs from 400 to 750 m upon comparing with the observations used in this paper (Tab. 4.1). The total of geostrophic and Ekman transport is estimated to be 8.9±1.7 Sv, where the latter is computed from two wind products: from the National Centers for Environmental Prediction, NCEP1 on a $2° \times 2°$ grid and the Quick Scatterometer (QuickSCAT) winds on a $1° \times 2°$ grid. Thus, Ekman transport of 3.7±0.7 Sv contributes 42% of total transport. Given this ratio, the geostrophic component would comprise roughly 58% of total transport. Applying this to the model, 58% of -11.51 Sv is only -6.70 Sv which is still higher by a couple of Sverdrups than the observed -4.88 Sv geostrophic transport. Thus, the model is overestimating the transport in the upper 400 m.

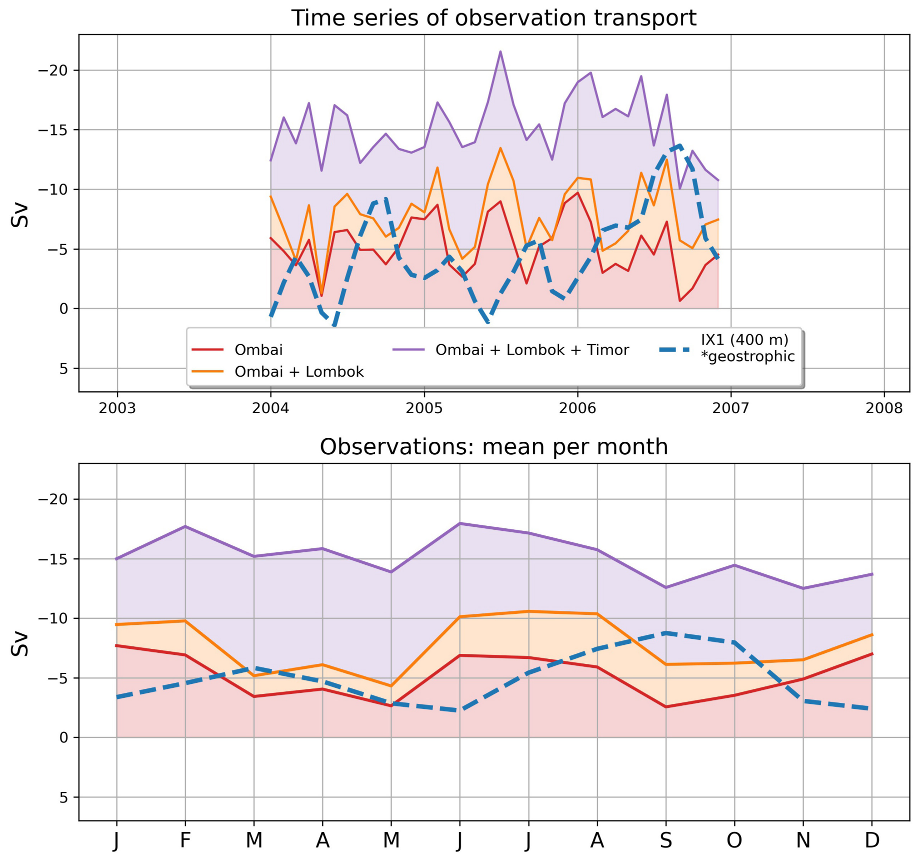

Figure 4.6: The IX1 geostrophic transport until 400 m is compared with the sum of total observed transport in Ombai Strait, Lombok Strait, and Timor Passage. (top) A time series from 2004 to 2007 and (bottom) monthly averages.

4.1.4 Comparison of transport through the outflow passageways and across the IX1 line

The expectation is that the transport from the outflow passageways approximates the total ITF transport. Similarly, the total IX1 transport is used by many previous studies as a proxy for total ITF transport. Thus, the IX1 transport should match the sum of the transport from the outflow passageways.

The observations from the three outflow passageways Ombai Strait, Lombok Strait, and Timor Passage are shown in comparison with the IX1 geostrophic transport from the top 400 m (Fig. 4.6). The discrepancy between the summed transport of the three passageways and the IX1 is large: the average of the three outflow passages is -15.13 Sv while the mean IX1 geostrophic transport in the top 400 m is -4.88 Sv. Given total transport through the three passageways averaging -15.13 Sv, the estimates of 8.9 Sv total transport in the top 750 m (S. E. Wijffels et al., 2008) leaves

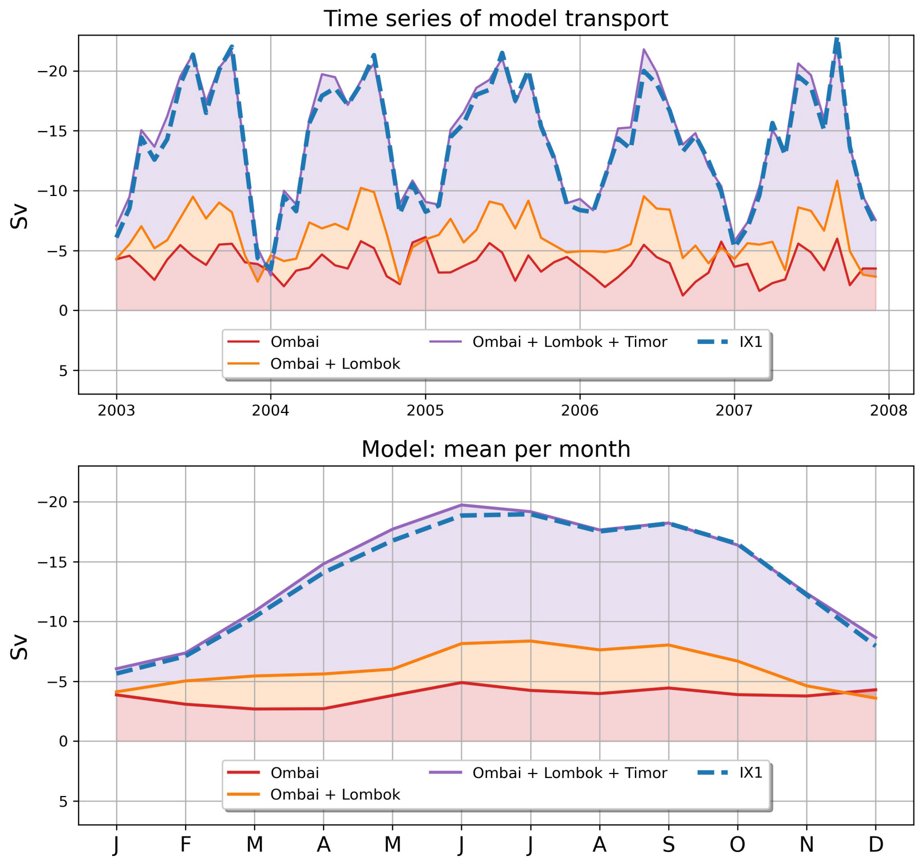

Figure 4.7: The modelled 1960-2015 IX1 total transport (full depth) is compared with the sum of total transport in Ombai Strait, Lombok Strait, and Timor Passage. (top) A sample of the time series from 2003 to 2008 and (bottom) monthly averages.

approximately 6 Sv that might be transported below 750 m.

The modelled IX1 total transport averages -13.68±5.3 Sv for the full depth and -11.51 Sv from 0-400 m, with a 2.17 Sv difference. This implies that little transport is seen below 400 m in the model, and thus the IX1 transport in the upper vertical layers may be overestimated while the lower transport is underestimated.

Indeed, in the model, we show (Figs. 4.7 and 4.8) that the modelled total transports in Ombai Strait, Lombok Strait, and Timor Passage add up to the total transport across the IX1 line. The result of a Pearson-r correlation of the sum of the three outflow passageways and the total IX1 transport is 0.9939 for the years 1960-2015 and and 0.9949 for the years 2070-2100. In summary, the model is self-consistent because the sum of the transport at the outflow passageways matches that of the IX1. Because the individual outflow passageways match the observations well in terms of yearly averages, the modelled IX1 total is a reliable proxy for the total ITF transport.

In terms of magnitude, the total transport is within the lower range of CMIP5

Figure 4.8: The modelled 2070-2100 IX1 total transport is compared with the sum of total transport in Ombai Strait, Lombok Strait, and Timor Passage. (top) A sample of the time series from 2090 to 2095 and (bottom) monthly averages.

models. In Stellema et al., 2019, the mean transport shallower than 1500 m was -13 Sv with an interquartile range from -12 to -16 Sv based on 28 models. In Santoso et al., 2022, the multi-model mean was -15.3 Sv for 20 CMIP5 models. These two studies computed the model transport across transects connecting the island of Java to northwestern Australia. Both were westward of Ombai Strait and Timor Sea, towards the Indian Ocean (Fig. 2.1).

4.1.5 Predicted transport during future conditions

From 2070–2100, the transport among all the transects is lower than the transport from 1960–2015 (Tab. 4.1). For Timor Passage, the transport falls by 1.57-4.95 Sv with the largest difference in March and smallest in November (4.2). In the months of January (+0.49 Sv) and February (+0.55 Sv), the transport is towards the Pacific. For Lombok Strait, the slowdown is weakest among all transports ranging from 0.11 to 1.00 Sv. In December, the future transect even exceeds the current transport by

0.32 Sv (4.3). For Ombai Strait, the weakening of the transport ranges from 1.55 to 3.46 Sv: the 1960–2015 average is -3.80 Sv while the 2070-2100 is -1.19 Sv (4.4). Lastly, across the IX1, the weakening of the top 400 m ranges from 1.40 to 4.80 Sv (Fig. 4.5) for the period 2070-2100.

Multi-model averages have consistently shown a projected decline in the ITF which is not associated with wind-driven circulation (M. Feng et al., 2017). Instead, it is hypothesised to be caused by reduced deep water formation in the Southern Ocean and decreased upwelling in the deep Pacific Ocean. M. Feng et al., 2017 revised the Island Rule to include a term representing the contribution of deep upwelling in the Pacific. With this amendment, the Island Rule captured the ITF better in terms of interannual, decadal and centennial changes as confirmed by the results of eddy-resolving models. The multi-model median of 28 CMIP5 climate models is an ITF weakening of 3-4 Sv by 2100 in the RCP8.5 scenario (Stellema et al., 2019). In comparison, the full transport across the IX1 slows down by $\sim$5.90 Sv which is higher than the mean of CMIP5 models.

4.2 ONI and IOD in the iHESP CESM1.3 model

On interannual timescales, the ITF transport is heavily influenced by the ENSO and IOD (Clarke and Liu, 1994, Meyers, 1996, Gordon et al., 1999, Sprintall and Révelard, 2014, Potemra and Schneider, 2007). Thus, we will look at their relationship but first, how well are the observed indices captured by the model? The ENSO phases tend to be longer in the model and weaker in amplitude (Fig. 4.9). Monthly standard deviation of the ONI is used as a proxy for its activity: based on the observations, the most active month is December and least active is May. The model's amplitude is weaker: its active month, January, is almost 0.3°C less than the peak of the observations. This peak is shifted late compared with observations, and so is the least active month of July which is $\sim$0.05°C higher than the May trough of the observations. Shown in the bottom plot are the time series in the frequency domain, after a Fourier transform is applied. ENSO cycles in the observations are more frequent and shorter than in the model, where the spectral peak of the observations corresponds to 1 ENSO cycle per 3.6 years ($\sim$2.8 cycles per decade) whereas the model's peak is at 1 ENSO cycle per $\sim$6.5 years ($\sim$1.5 cycles per decade). This shortcoming of the model is acknowledged in the iHESP paper Chang et al., 2020.

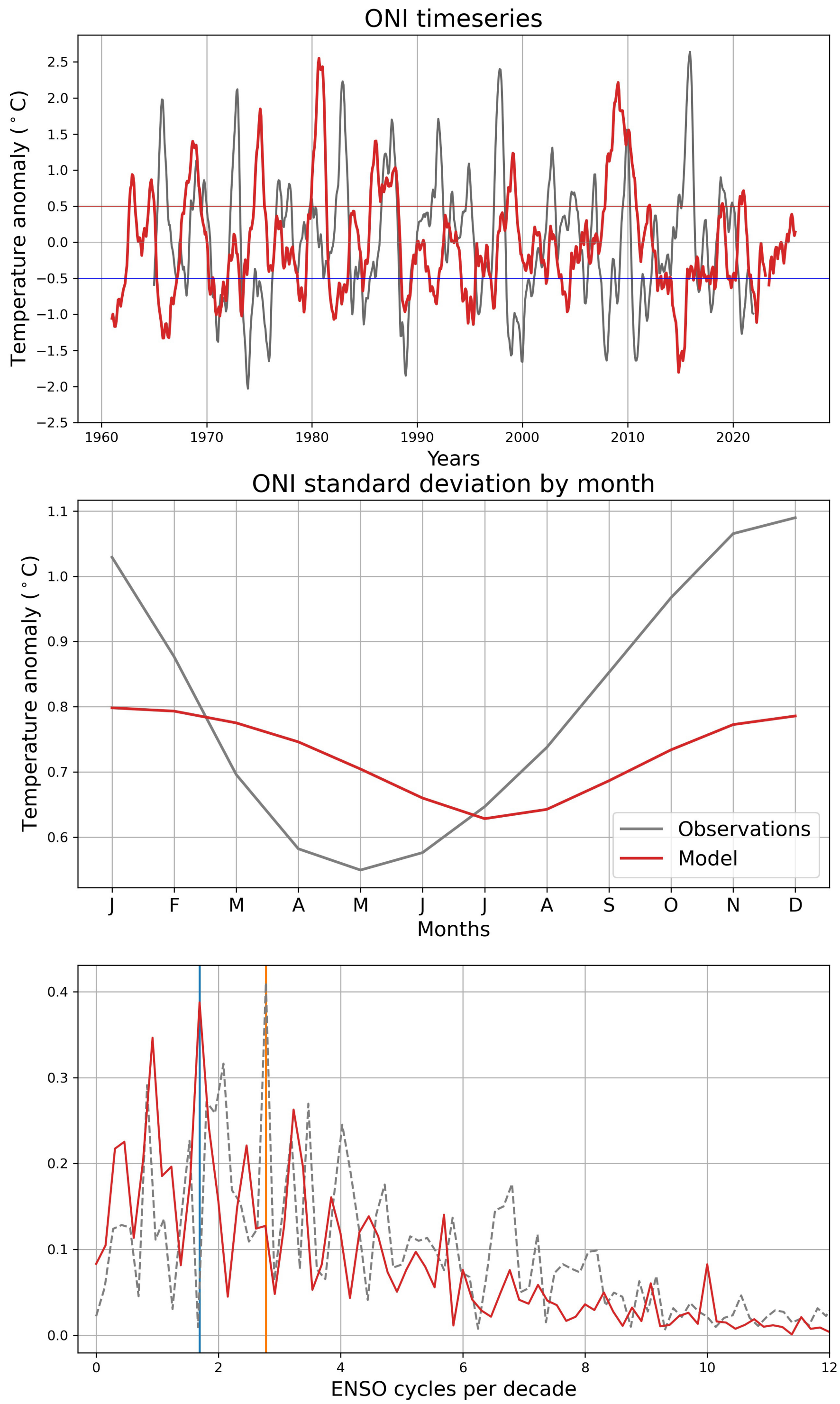

Figure 4.9: Grey lines correspond with the Oceanic Niño Index in observations and red corresponds with the model. (top) The blue and red horizontal lines indicate -0.5 and 0.5°C: La Niña or El Niño, respectively, occurs if the ONI exceeds these values for 5 months. (middle) One standard deviation for each month. (bottom) The two time series in the frequency domain, after a Fourier transform is applied, with the blue line showing the highest peak of the model and the orange line marking the highest peak of the observations.

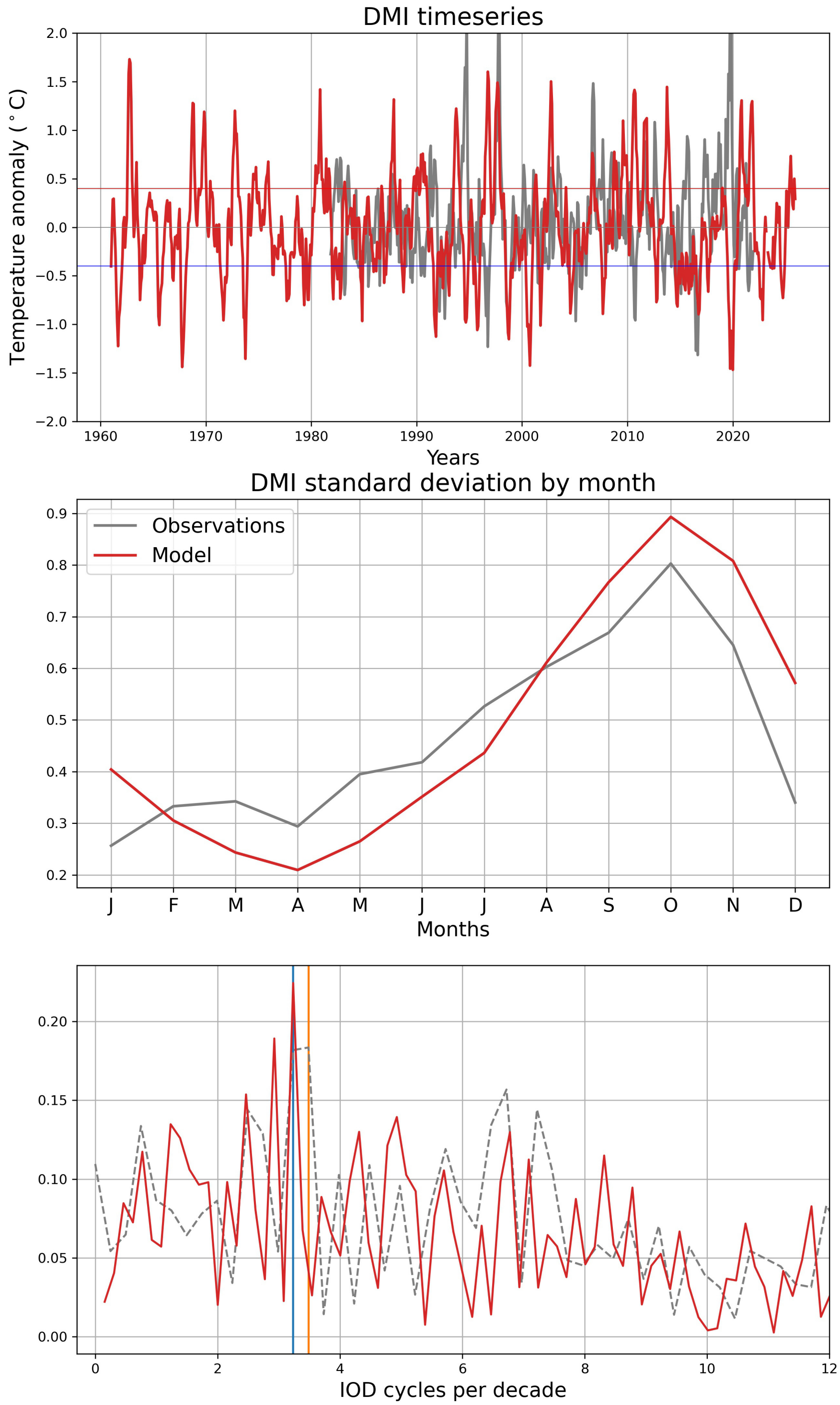

Figure 4.10: Grey lines correspond with the Dipole Mode Index in observations and red corresponds with the model. (top) The blue and red horizontal lines indicate -0.4 and 0.4°C: a negative or positive event, respectively, occurs if the DMI exceeds these values for 3 months. (middle) One standard deviation for each month. (bottom) The two time series in the frequency domain, after a Fourier transform is applied, with the blue line showing the highest peak of the model and the orange line marking the highest peak of the observations.

The DMI timeseries is noisier than the ONI because by definition, the latter is based on the 3-month mean of SSTA while in the former, no such averaging is applied. Based on the middle plot (Fig. 4.10), the activity of the DMI is captured well, given that the monthly average magnitudes are similar: the peaks are both in October and less than 0.1°C apart. The lowest point of the observational monthly average is in January and a secondary trough appears in April. The model's minimum is in April which is < 0.1°C less than the January or April troughs of the observations. The time series in spectral space shows a good correspondence of the observations and model whose peaks are at one DMI cycle per ∼2.9 years (∼3.5 cycles per decade) and one DMI cycle per ∼3.3 years (∼3.08 cycles per decade), respectively. Unlike the ENSO cycle, the IOD was not discussed in the iHESP paper Chang et al., 2020.

4.3 ITF relationships with ENSO and IOD

By convention, a more negative ITF means a stronger flow towards the Indian Ocean. A positive correlation with the ONI means that the ITF transport is behaving as expected with respect to ENSO. First, it can mean that the ONI is positive which is an El Niño meaning less transport and thus a positive anomaly. Second, a positive correlation also results from a negative ONI or La Niña meaning more transport and thus a negative ITF transport anomaly.

4.3.1 Lead-lag analysis of IX1 transport with ENSO and IOD phases

The IX1 transport is used in this section as a proxy for total ITF transport. At 0 months lag, the IX1 transport correlates best and significantly with ONI values from July to November with correlation values of 0.4–0.6, using a Pearson-r correlation and its corresponding two-tailed p-value. The strongest transport of the IX1 occurs in from June to September (Fig. 4.5). The strongest, significantly positive correlations occur in the July to November months of the IX1 transport. The July transport correlates with the ONI from the July of the previous year until March of the next year, 21 consecutive months of significant correlations. However, for IX1 transport anomaly in August the significant correlations begin in January of the year before; for September, the January of the year before; and for October, the February of the year before. The beginning months of these correlations roughly corresponds with the peaking of the ENSO signal which peaks from November to February (Fig. 4.9). For

August to October, beginning months are also 7–8 months lagged from the ENSO peak which corresponds with the expected travel time of the Pacific Rossby and subsequent coastal Kelvin waves. The correlation remains high up to 8–11 months afterwards and that is likely because ENSO phases last months to years: the ENSO events which happen in the present will be correlated with the ENSO in the succeeding months.

During March, June, and December, the IX1 does not correlate strongly or significantly with ENSO. There are some significant correlations in the months January, February, March, and April. In March and April, the IX1 correlates negatively with ENSO meaning that the effect opposite to expected occurs where we would see a strengthening during El Niño or weakening during La Niña; while from January to March, the IX1 correlates with ENSO signals in the future.

Before performing such an analysis on the IOD, the ENSO signal is removed using a linear regression. In a previous study by H. Liu et al., 2005, the removal of the ENSO signal was attempted and the correlation of the IOD with ITF transport was insignificant. Specifically, the ENSO signal was subtracted from the IOD signal using a simple linear regression and the correlation was 0.07 with the residual IOD signal and the IX1 transport, the former leading by four months. This study utilised a quasi-global eddy permitting oceanic general circulation model, LICOM1.0 (State Key Laboratory of Numerical Modeling for Atmospheric Sciences and Geophysical Fluid Dynamics/Institute of Atmospheric Physics Climate system Ocean Model version 1.0) with $0.5^\circ \times 0.5^\circ$ resolution.

Given that the ENSO correlates best with ITF transport during the months July to October (Fig. 4.11), a simple linear regression is performed on the IX1 transport and ONI from these months, with a resulting R^2 value of 0.508 (Fig. 4.12). The residual ITF transport anomaly is calculated with the linear relationship subtracted despite the low R^2 value, and then correlated with the DMI (Fig. 4.13).

For the IOD, a negative correlation yields the expected results because during a positive IOD phase, more transport is expected and therefore produces a negative anomaly and during a negative IOD phase, less transport is expected and therefore results in a positive anomaly. Overall, the residual IX1 transport anomaly does not significantly correlate with the DMI within the expected months. The IOD is expected to lead the IX1 by 0–5 months (Sprintall et al., 2009, S. Wijffels and Meyers, 2004). For an IOD leading the ITF transport by 0–5 months, the correlations are primarily negative; however, the absolute value of all these correlation values is < 0.20 and insignificant. The significant correlations appear with DMI more than five months

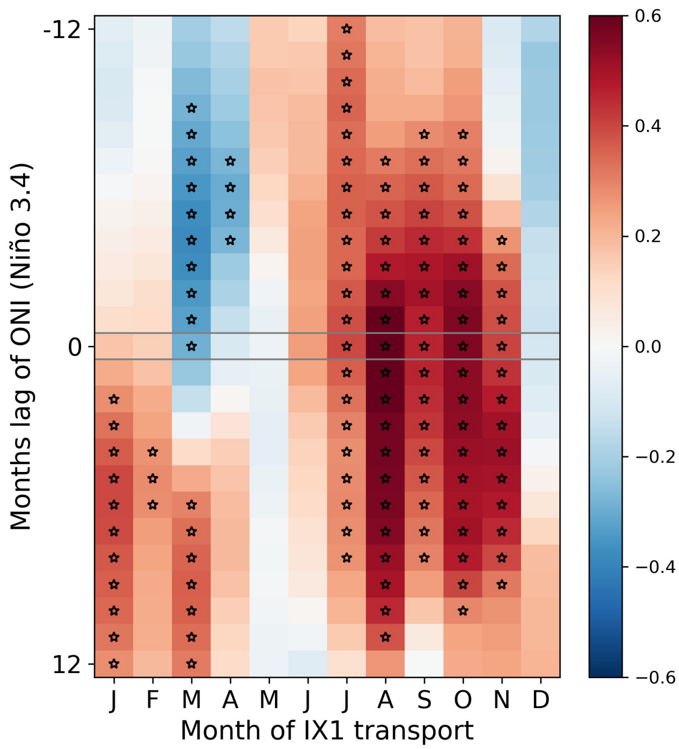

Figure 4.11: A lead-lag correlation of ONI strength, computed from the model, from 12 months before to 12 months after IX1 transport. A positive lag means that the ENSO occurs after the IX1. Significant correlations, with p-values less than 0.05, are marked with stars.

before the current IX1 month and significant positive correlations with the DMI 9 months in the future.

4.3.2 Transport categorised by ENSO and IOD phase

The model output is categorised by ENSO and IOD phase (Tab. 4.2). A year is designated as a positive or negative ENSO if the anomaly occurs in its most active months, November to February (Fig. 4.9). The same procedure is performed with the IOD, whose most active months are from September to November (Fig. 4.10). If no ENSO occurs during these months, it is considered ENSO neutral and likewise with the IOD. For a certain ONI and DMI combination of phases, the corresponding transport average was taken from July to September of the next year (Fig. 4.14) because the ENSO correlated best with the IX1 transport during the months from July to October (Fig. 4.11).

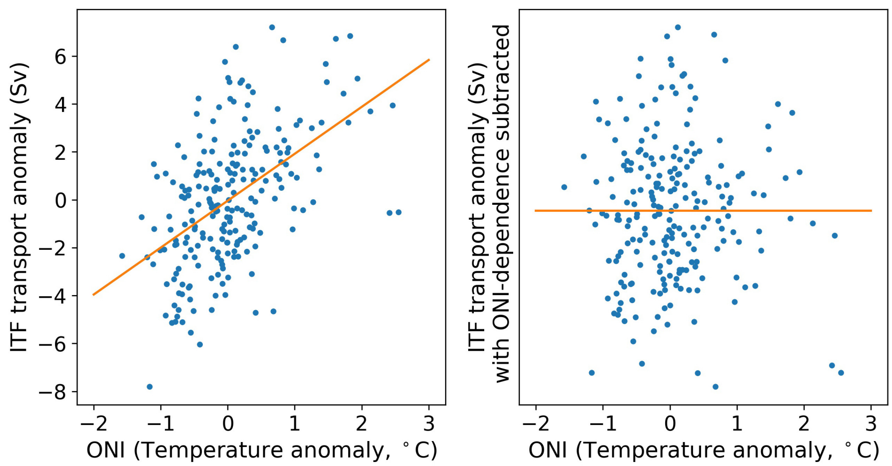

Figure 4.12: (left) Linear fit of July-August-September-October ONI and IX1 transport, with an R^2 value of 0.508 and line equation of $y = 1.96x - 0.039$. (right) The residual IX1 transport against the same ONI values, with the line subtracted.

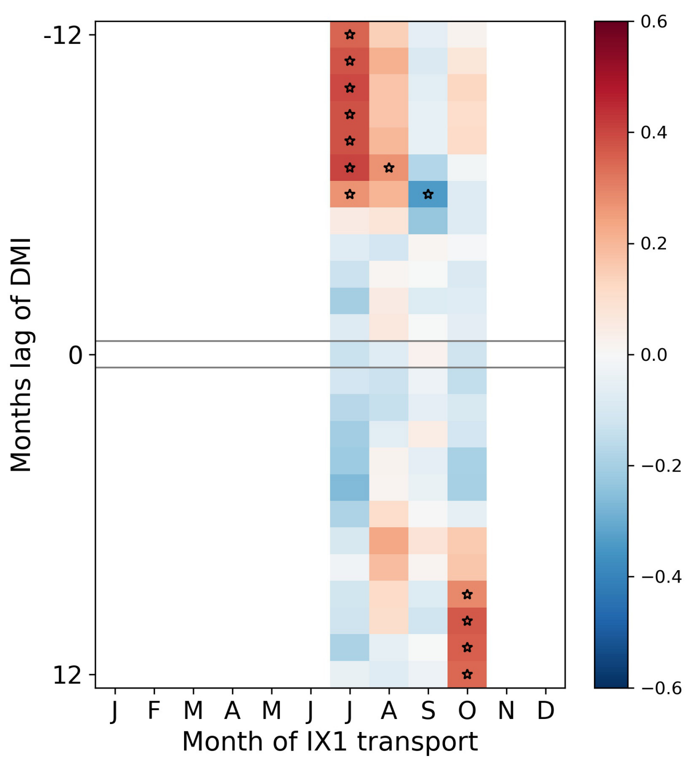

Figure 4.13: (left) A lead-lag correlation of IOD strength for the months July, August, September, and October IX1 transport from which the linear dependence of the ONI was subtracted.

	(-) IOD	IOD neutral	(+) IOD
(+) ENSO	1967, 1998, 2007	1964, 1985, 1986, 2008	1968, 1974, 1980, 1987, 2009
ENSO neutral	1963, 1973, 1976, 1983, 1995, 2000, 2001, 2004	1977, 1979, 1984, 1989, 1992, 1999, 2005, 2012	1962, 1969, 1972, 1975, 1990, 1993, 1997, 2002, 2006, 2010, 2011, 2013
(-) ENSO	1961, 1965, 1971, 1988, 1991, 1994, 2014	1966, 1970, 1978, 1981, 1982, 2003	1996

Table 4.2: Years from 1961–2014 of model output categorised by ENSO and IOD phase. The bars indicate standard error.

Positive ENSO phases often occur with positive IOD phases, where the former causes weakened transport which by convention, is a positive transport anomaly and the latter causes the opposite, a negative anomaly. Thus, their effects can counteract each other. When both are positive, with the exception of Makassar Strait, we see no significant transport and these climate indices do not seem to have much of an effect. A positive ENSO occurs with a negative IOD phase in three years of the model output (Tab. 4.2) and all the transports are weakened, as represented by positive transport anomalies: this corresponds with the theoretical expectation that the effects of that positive ENSO and negative IOD phases both work to weaken the ITF transport. Specifically, the IX1, Timor Passage, and Lombok Strait are significantly strengthened. Meanwhile, Makassar and Ombai Straits transports are within the significant error bars and therefore are not significantly strengthened. During the IOD neutral phases which coincide with positive ENSO, the transport weakens in all transects except Makassar Strait which strengthens. The weakening is significant for the IX1 and Timor Passage. The strengthening of the Makassar Strait transport is not significant, although the expectation is that it would weaken.

Among the ENSO neutral years, the expectation is that the IOD effects would be significant but in fact, they are not. During the ENSO neutral and IOD negative years, the transport across all the transects is weakened as expected, however all are less than 0.5 Sv and not significant. During IOD neutral years, the transport is strengthened but not significantly. During IOD positive years, we expect a strengthening of the transport in the straits and only see an insignificant strengthening in Lombok Strait, and the rest of the transects were weakened contrary to expectations. In fact, the Makassar Strait is significantly strengthened by 0.6 Sv. This may be due to the 11 month lag from the beginning of the IOD phase: the DMI leads ITF transport by 0-5 months and the choice of July to September months prioritised the ENSO lag of 9 months. Additionally, the ENSO effect was more prominent (Fig. 4.11 versus Fig. 4.13), especially since the ENSO lasts longer and has a larger spatial scale.

The transport from other quarters of the year were tested using this analysis. For example, we chose a three-month window that is 3 months lagged from the beginning of the IOD peak, September: July to September transport was categorised into the different IOD and ENSO phases, in this same analysis (not shown). The motivation was to see if the effects of the IOD would be significant. However, the results for positive and negative IOD phases remained insignificant: no significant weakening during a negative IOD and no significant strengthening during a positive IOD. Similar to the lead-lag correlation (Fig. 4.13), it may be difficult to find any DMI effects on ITF transport in this model.

Lastly, the ITF transport during La Niña phases is mostly enhanced, corresponding with expectations. A La Niña only co-occurred with a positive IOD phase in 1996 and thus data from this year is excluded. During negative IOD phases, its effects are expected to counteract the La Niña: the IX1 and Timor Passage are significantly enhanced while Makassar Strait, Lombok Strait, and Ombai are not. During neutral IOD phases, the La Nina effect of strengthening transport is significant in the IX1, Makassar Strait, and Timor Passage, insignificant in Ombai Strait, and slightly weakened in Lombok Strait.

In several categories of ENSO and IOD phase, the Makassar Strait (Fig. 4.14) differs from the expected behaviour: e.g., it is significantly strengthened during positive ENSO and positive IOD years when we expect that it should be weakened because the ENSO signal would dominate. We have two theories about why the Makassar Strait may act differently. First, it is an inflow passage or upstream in comparison with the four other transects, and thus would receive ENSO signals earlier. Therefore, the imposed lag of 8 months is likely too much for Makassar. Second, freshwater buoyancy forces may be at play. Gordon et al., 2012 ran a global HYCOM model with a resolution of $1/12.5° \times 1/12.5°$ where they found that freshwater can enter the South China Sea Throughflow through the Mindoro-Sibutu Passage. A west-to-east pressure gradient is formed which can inhibit the surface Mindanao-Sulawesi inflow into the Makassar Strait. Freshwater "plugs" can inhibit near-surface southerly flow and transport in the Makassar Strait.

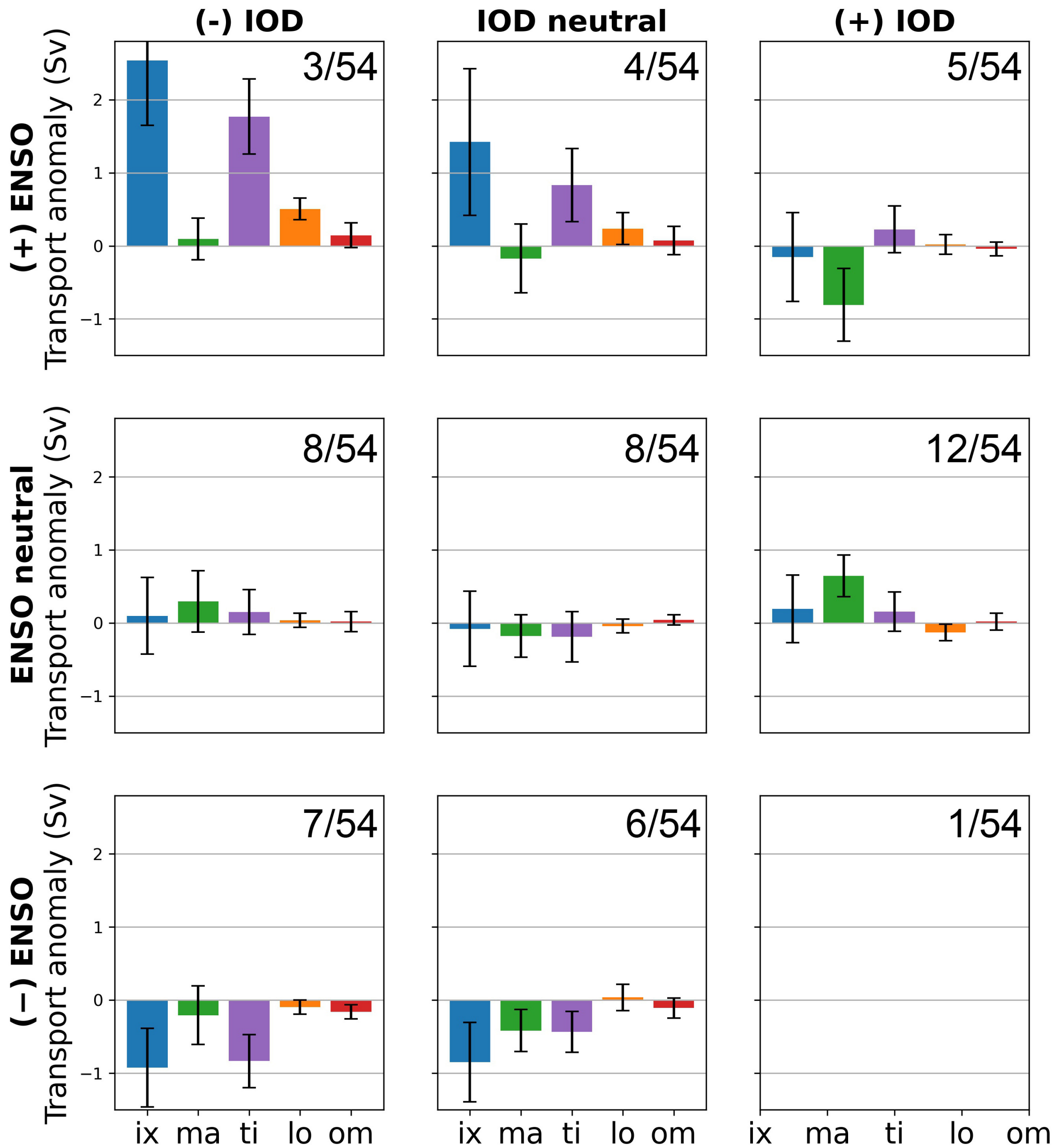

Figure 4.14: Transport anomaly bar graph per transect with respect to ONI and ENSO positive, neutral, and negative phases. The IX1 transect is labelled "ix", Makassar Strait as "ma", Timor Passage as "ti", Lombok Strait as "lo", and Ombai Strait as "om". Numbers on the top right indicate the number of years in that category, out of 54 years in total.

Chapter 5

Summary and conclusion

The performance of the iHESP CESM1.3 model in capturing the transport of the ITF has been described in great detail. In this study, five transects were used. The first is an inflow passageway which is expected to carry 77% of the total ITF transport, the Makassar Strait (Gordon et al., 2019). The model underestimates the transport by 2.51 to 4.60 Sv, with the highest underestimations during December to February, or boreal winter. Nonetheless, from April to November, there are overlaps between the error bars of the monthly means of the observations and the model output. Therefore, the model captures the observed transport well except in winter where its underestimations are heaviest.

The transport through Timor Passage, Lombok Strait, and Ombai Strait are captured well by the model. These three make up the outflow passageways. For the Timor Passage, the model overestimated transport during boreal summer and underestimated transport during boreal winter, but the average yearly transport in the model (-7.97±3.68 Sv) is very close to that of observations (-7.36±2.15 Sv). The modelled transport yearly averages (-2.30±1.67 Sv) and observations (-2.60±1.42 Sv) are even closer in Lombok Strait. For the Ombai Strait, the transport is underestimated by the model by 1.38 Sv, especially the peaks in boreal summer and winter. However, overall the model captures the transport of the outflow passageways well despite these shortcomings.

The sum of the outflow straits is expected to match the total ITF transport. Similarly, the total transport across the IX1 line is expected to match the total ITF transport. The model is self-consistent as the total IX1 transport indeed matches the total transport at the outflow passageways (Figs. 4.7 and 4.8). Thus, we can trust the IX1 total transport to be a proxy of ITF total transport since the individual outflow passageways matched observations well.

There remains a large discrepancy between modelled IX1 transport in the upper 400 m and the observed geostrophic transport (also 0-400 m). We hypothesise that this can be accounted for mostly by the lack of Ekman transport in the observations, model overestimations of the top 400 m, and underestimations of transport below 400 m. Nonetheless, the modelled total transport of the IX1 matches excellently with the modelled total transport at the outflow straits: therefore, discrepancy with the observations does not invalidate it as a proxy for total ITF transport.

It is hypothesised that in a warming world, more El Niño-like conditions are expected as well as the decreased upwelling in the deep Pacific Ocean (M. Feng et al., 2017), causing the ITF to slow down. We see from the results that across all transects, the transport is weakened in the future. If we take the IX1 as a proxy for the whole ITF transport, its decrease is approximately 6 Sv. In comparison with the multi-model median of 3-4 Sv in 28 CMIP5 climate models (Stellema et al., 2019), the weakening of the iHESP CESM1.3 model is too strong in comparison. Nonetheless, the model used in this study captures the general trend of a weakening ITF.

The ENSO effects are strongest on the IX1 transport from July to November, with significant correlation values of 0.4-0.6. Significantly high correlations with IX1 transport in August to October begin during the peak of the ENSO, November of the year before to February (Fig. 4.5). For these months, the transport responds as expected to the ENSO phase: weakening (strengthening) during El Niño (La Niña).

Using a linear regression, the ENSO signal is removed from the IX1 transport during the months of July to October, the months which correlate best with ENSO. The DMI is expected to lead the ITF transport by 0-5 months (Sprintall et al., 2009, S. Wijffels and Meyers, 2004). During these months, the residual IX1 transport correlates negatively with the IOD phase as expected: the transport during a negative (positive) IOD phase is weakened (strengthened) and therefore we have a positive (negative) transport anomaly. However, these correlations within the expected months are not significant and thus the effects of the IOD are not conclusively present.

Corresponding to the months with the highest correlations with ENSO, July to September transports for each transect were categorised by ENSO and IOD phase (Fig. 4.14). The El Niño effect of weakening the flow is seen across all transects, especially when it coincides with a negative IOD phase which has the same effect. When a positive ENSO phase coincides with a neutral IOD phase, the transport is weakened but not as much. La Niña effects to strengthen the flow are seen in all transects. The effects are usually significant across the IX1 line and Timor Passage. Meanwhile, the Makassar Strait may act differently because it's an inflow passage or freshwater buoyancy forces may affect its transport. The IOD effects during ENSO neutral years are not significant. Thus, we have not successfully demonstrated any statistically significant IOD influence on ITF transport; however, the ENSO effects to weaken or strengthen the flow are confirmed in this model.

Global climate models are aiming for higher and higher resolution. More models in the future will be able to resolve the major passageways of the Indonesian Throughflow. Thus, future work might compare the results from this high resolution run with that of the iHESP CESM1.3 lower resolution run to see if there was an improvement in the modelling of the total ITF transport, in the process of increasing resolution. Other immediate tasks would be to investigate this model's vertical profiles of transport. Lastly, it would be interesting to investigate how well this iHESP CESM1.3 model captures other variables such as sea surface temperatures which are important to upwelling, air-sea fluxes and currents, sea surface salinity which affects density-driven circulation, and mixed layer depth which is a proxy for turbulent mixing processes.

References

Australian Research Data Commons. (2022). IMOS SOOP-XBT Upper Ocean Thermal Data collected on the line IX1 (Fremantle-Sunda Strait) [Online; accessed 27-May-2022].

Bray, N. A., Hautala, S., Chong, J., & Pariwono, J. (1996). Large-scale sea level, thermocline, and wind variations in the indonesian throughflow region. *Journal of Geophysical Research: Oceans*, *101*(C5), 12239–12254.

Chang, P., Zhang, S., Danabasoglu, G., Yeager, S. G., Fu, H., Wang, H., Castruccio, F. S., Chen, Y., Edwards, J., Fu, D., et al. (2020). An unprecedented set of high-resolution earth system simulations for understanding multiscale interactions in climate variability and change. *Journal of Advances in Modeling Earth Systems*, *12*(12), e2020MS002298.

Clarke, A. J., & Liu, X. (1994). Interannual sea level in the northern and eastern indian ocean. *Journal of Physical Oceanography*, *24*(6), 1224–1235.

England, M. H., & Huang, F. (2005). On the interannual variability of the indonesian throughflow and its linkage with enso. *Journal of Climate*, *18*(9), 1435–1444.

Feng, M., Zhang, X., Sloyan, B., & Chamberlain, M. (2017). Contribution of the deep ocean to the centennial changes of the indonesian throughflow. *Geophysical Research Letters*, *44*(6), 2859–2867.

Feng, X., Liu, H., Wang, F., Yu, Y., & Yuan, D. (2013). Indonesian throughflow in an eddy-resolving ocean model. *Chinese Science Bulletin*, *58*(35), 4504–4514.

Ffield, A., & Gordon, A. L. (1992). Vertical mixing in the indonesian thermocline. *Journal of Physical Oceanography*, *22*(2), 184–195.

Godfrey, J. (1996). The effect of the indonesian throughflow on ocean circulation and heat exchange with the atmosphere: A review. *Journal of Geophysical Research: Oceans*, *101*(C5), 12217–12237.

Gordon, A. L., & Fine, R. A. (1996). Pathways of water between the pacific and indian oceans in the indonesian seas. *Nature*, *379*(6561), 146–149.

Gordon, A. L., Huber, B. A., Metzger, E. J., Susanto, R. D., Hurlburt, H. E., & Adi, T. R. (2012). South china sea throughflow impact on the indonesian throughflow. *Geophysical Research Letters*, *39*(11).

Gordon, A. L., Napitu, A., Huber, B. A., Gruenburg, L. K., Pujiana, K., Agustiadi, T., Kuswardani, A., Mbay, N., & Setiawan, A. (2019). Makassar strait throughflow seasonal and interannual variability: An overview. *Journal of Geophysical Research: Oceans*, *124*(6), 3724–3736.

Gordon, A. L., Sprintall, J., Van Aken, H. M., Susanto, D., Wijffels, S., Molcard, R., Ffield, A., Pranowo, W., & Wirasantosa, S. (2010). The indonesian throughflow during 2004–2006 as observed by the instant program. *Dynamics of Atmospheres and Oceans*, *50*(2), 115–128.

Gordon, A. L., Susanto, R. D., & Ffield, A. (1999). Throughflow within makassar strait. *Geophysical Research Letters*, *26*(21), 3325–3328.

iHESP. (2022a). iHESP data release - Phase 2 [Online; accessed 24-May-2022].

iHESP. (2022b). Models [Online; accessed 24-May-2022].

Ilahude, A. G., & Gordon, A. L. (1996). Thermocline stratification within the indonesian seas. *Journal of Geophysical Research: Oceans*, *101*(C5), 12401–12409.

Lee, T., & McPhaden, M. J. (2008). Decadal phase change in large-scale sea level and winds in the indo-pacific region at the end of the 20th century. *Geophysical Research Letters*, *35*(1).

Liu, H., Li, W., & Zhang, X. (2005). Climatology and variability of the indonesian throughflow in an eddy-permitting oceanic gcm. *Advances in Atmospheric Sciences*, *22*(4), 496–508.

Liu, Q.-Y., Feng, M., Wang, D., & Wijffels, S. (2015). Interannual variability of the indonesian throughflow transport: A revisit based on 30 year expendable bathythermograph data. *Journal of Geophysical Research: Oceans*, *120*(12), 8270–8282.

Meehl, G. A., Yang, D., Arblaster, J. M., Bates, S. C., Rosenbloom, N., Neale, R., Bacmeister, J., Lauritzen, P. H., Bryan, F., Small, J., et al. (2019). Effects of model resolution, physics, and coupling on southern hemisphere storm tracks in cesm1. 3. *Geophysical Research Letters*, *46*(21), 12408–12416.

Meyers, G. (1996). Variation of indonesian throughflow and the el niño-southern oscillation. *Journal of Geophysical Research: Oceans*, *101*(C5), 12255–12263.

Potemra, J. T., & Schneider, N. (2007). Interannual variations of the indonesian throughflow. *Journal of Geophysical Research: Oceans*, *112*(C5).

Ridgway, K., Thresher, A., Roemmich, D., Sutton, P., Ball, G., & Cowen, L. (2013). Extend high-density XBT sections sampling the main currents around Australia [Online; accessed 27-May-2022].

Saji, N., Goswami, B. N., Vinayachandran, P., & Yamagata, T. (1999). A dipole mode in the tropical indian ocean. *Nature*, *401*(6751), 360–363.

Samanta, D., Goodkin, N. F., & Karnauskas, K. B. (2021). Volume and heat transport in the south china sea and maritime continent at present and the end of the 21st century. *Journal of Geophysical Research: Oceans*, *126*(9), 1–28.

Santoso, A., England, M. H., Kajtar, J. B., & Cai, W. (2022). Indonesian throughflow variability and linkage to enso and iod in an ensemble of cmip5 models. *Journal of Climate*, *35*(10), 3161–3178.

Song, Q., Gordon, A. L., & Visbeck, M. (2004). Spreading of the indonesian throughflow in the indian ocean. *Journal of Physical Oceanography*, *34*(4), 772–792.

Sprintall, J., & Révelard, A. (2014). The indonesian throughflow response to indopacific climate variability. *Journal of Geophysical Research: Oceans*, *119*(2), 1161–1175.

Sprintall, J., Wijffels, S. E., Molcard, R., & Jaya, I. (2009). Direct estimates of the indonesian throughflow entering the indian ocean: 2004–2006. *Journal of Geophysical Research: Oceans*, *114*(C7).

Stellema, A., Sen Gupta, A., & Taschetto, A. S. (2019). Projected slow down of south Indian Ocean circulation. *Scientific reports*, *9*(1), 1–15.

Tokinaga, H., Xie, S.-P., Timmermann, A., McGregor, S., Ogata, T., Kubota, H., & Okumura, Y. M. (2012). Regional patterns of tropical indo-pacific climate change: Evidence of the walker circulation weakening. *Journal of Climate*, *25*(5), 1689–1710.

Trenberth, K. & National Center for Atmospheric Research Staff (Ed.). (2020). The Climate Data Guide: Nino SST Indices (Nino 1+2, 3, 3.4, 4; ONI and TNI) [Online; accessed 24-May-2022].

Wang, C. (2019). Three-ocean interactions and climate variability: A review and perspective. *Climate Dynamics*, *53*(7), 5119–5136.

Wijffels, S., & Meyers, G. (2004). An intersection of oceanic waveguides: Variability in the indonesian throughflow region. *Journal of Physical Oceanography*, *34*(5), 1232–1253.

Wijffels, S. E., Meyers, G., & Godfrey, J. S. (2008). A 20-yr average of the indonesian throughflow: Regional currents and the interbasin exchange. *Journal of Physical Oceanography*, *38*(9), 1965–1978.

Wyrtki, K. (1987). Indonesian through flow and the associated pressure gradient. *Journal of Geophysical Research: Oceans*, *92*(C12), 12941–12946.

Wyrtki, K. (1961). *Physical oceanography of the southeast asian waters* (Vol. 2). University of California, Scripps Institution of Oceanography.

Yuan, Y., & Li, C. (2008). Decadal variability of the iod-enso relationship. *Chinese Science Bulletin*, *53*(11), 1745–1752.